Title

Room surface convective heat transfer with ceiling fans and its effect on radiant cooling systems

Journal

Journal of Building Performance Simulation

ISSN

1940-1493 1940-1507

Authors

Duarte Roa, Carlos
Raftery, Paul
Lee, Sangjoon
et al.

Publication Date

2026-04-15

DOI

10.1080/19401493.2026.2656928

Journal of Building Performance Simulation

ISSN: 1940-1493 (Print) 1940-1507 (Online) Journal homepage: www.tandfonline.com/journals/tbps20

Room surface convective heat transfer with ceiling fans and its effect on radiant cooling systems

Carlos Duarte Roa, Paul Raftery, Sangjoon Lee & Aslihan Senel Solmaz

To cite this article: Carlos Duarte Roa, Paul Raftery, Sangjoon Lee & Aslihan Senel Solmaz (15 Apr 2026): Room surface convective heat transfer with ceiling fans and its effect on radiant cooling systems, Journal of Building Performance Simulation, DOI: 10.1080/19401493.2026.2656928

To link to this article: https://doi.org/10.1080/19401493.2026.2656928

Published online: 15 Apr 2026.

JOURNAL OF BUILDING PERFORMANCE SIMULATION
https://doi.org/10.1080/19401493.2026.2656928

Taylor & Francis
by informa

Room surface convective heat transfer with ceiling fans and its effect on radiant cooling systems

Carlos Duarte Roa [a], Paul Raftery [a], Sangjoon Lee[b] and Aslihan Senel Solmaz[c]

[a]Center for the Built Environment, University of California, Berkeley, CA, USA; [b]Department of Aeronautics and Astronautics, Stanford University, Stanford, CA, USA; [c]Department of Architecture, Dokuz Eylul University, Izmir, Turkey

ABSTRACT

The integration of ceiling fans with radiant systems remains underexplored despite their potential to address cooling capacity limitations. This study adopts a two-step approach to quantify the impact of elevated air movement on thermally activated building systems (TABS). First, we used OpenFOAM to calculate convective heat transfer coefficients under varying airflows, air-to-surface temperature differences, and zone sizes. These coefficients also apply to ceiling fans in buildings without radiant systems. Second, we implemented these coefficients in EnergyPlus to evaluate key radiant design parameters. Scenario 1 results show median steady-state cooling heat transfer rates increase of up to 47% relative to the no-fan cases when operative temperature is held constant. Scenario 2 demonstrates a median cooling effect of up to 4.8 K under fixed capacity, reflecting both lower zone temperatures and direct air movement on occupants. Overall, TABS-fans systems offer a scalable strategy to enhance comfort, increase capacity, and reduce energy demand.

ARTICLE HISTORY
Received 15 September 2025
Accepted 1 April 2026

KEYWORDS
Radiant system; ceiling fans; convective heat transfer coefficient; CFD; energy simulation

Highlights

- We use CFD to develop simplified surface convective heat transfer models that account for air movement with ceiling fans on room surfaces.
- We use simplified surface convective models in EnergyPlus to evaluate radiant system performance with ceiling fans.
- Ceiling fans increase the zone's steady-state cooling heat transfer rate by a median of 47% at the highest fan speeds.
- Ceiling fans have a median cooling effect of up to 4.8 K at the highest fan speeds.
- A radiant and ceiling fan couple system has the potential to decrease HVAC energy use while maintaining occupant thermal comfort.

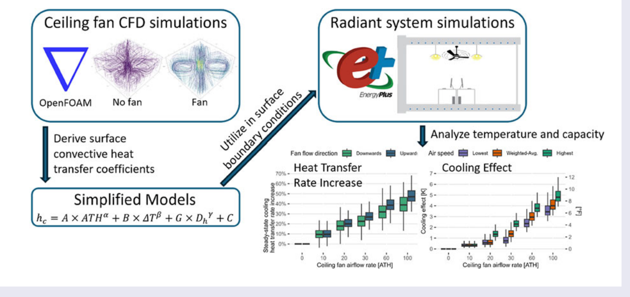

1. Introduction

Radiant heating and cooling systems are increasingly adopted as a strategy to reduce building energy use and greenhouse gas emissions compared to conventional all-air systems (Rhee and Kim 2015). This trend has accelerated in recent years as part of broader efforts to decarbonize buildings and enable low-temperature, high efficiency heating, ventilation, air conditioning (HVAC) operation (Carnieletto et al. 2024; Shindo et al. 2023; Shindo et al. 2024). They remove sensible cooling loads

CONTACT Carlos Duarte Roa cduarte@berkeley.edu

Supplemental data for this article can be accessed online at https://doi.org/10.1080/19401493.2026.2656928.

from the space by a combination of radiation and convection. While radiant heating is more common, radiant cooling systems are gaining traction, particularly in net-zero energy and high-performance buildings (Higgins and Carbonnier 2017). Recent demonstration projects and design guidance increasingly position radiant cooling as a core system rather than a niche application (Bauman et al. 2019). Hydronic radiant cooling systems operate at higher supply water temperatures than conventional systems, with relatively small temperature differences between the space and cooled surfaces (Duarte Roa et al. 2025).

The three main system types are radiant metal panels (RP), embedded surface systems (ESS), and thermally activated building systems (TABS) (Babiak, Olesen, and Petras 2009). ESS and TABS are high thermal mass radiant systems in which hydronic tubing is embedded in screed or structural concrete slabs, respectively (Raftery et al. 2017). These configurations have emerged as an economically and energetically efficient design strategy for both cooling and heating purposes (Gwerder et al. 2008). Their relevance has increased as buildings pursue load shifting, peak reduction, and grid-interactive operation. However, a widely cited drawback of radiant cooling is its limited cooling capacity (Olesen 1997). Ideally, this limitation is mitigated through an integrated design process that improves envelope design and reduces internal heat gains to the point that the radiant system can maintain comfortable conditions on the cooling design day without any supplemental cooling system. However, where this is not feasible, additional strategies are needed to increase system capacity and maintain thermal comfort. One promising approach is the use of elevated air movement, such as ceiling fans, to enhance convective heat transfer from cooled surfaces. Recent updates to comfort standards and renewed interest in ceiling fans as primary comfort devices have made this approach particularly timely (ASHRAE 2023; Kent et al. 2023; Miller et al. 2021). In addition to increasing system capacity, controlled air movement improves occupant thermal comfort by expanding the acceptable temperature range. This study focuses on evaluating the effects of ceiling fan induced air movement on TABS cooling performance through building performance simulation. Sources of elevated air movement such as ceiling fans also provide the added benefit of almost instantaneous control, which allows occupants to modify thermal comfort conditions far faster than systems that aim to condition the whole room, particularly so for radiant systems.

Several studies have examined the interaction between forced convection and radiant cooling systems. Jeong and Mumma (2003) developed correlations for mixed convection heat transfer on ceiling RP in a hypothetical space with nozzle diffusers near the ceiling. Their analysis suggested capacity gains of 5–35% depending on diffuser velocity (2–6 m s^{-1}) and chilled water temperature (12–25 °C). Similarly, Novoselac, Burley, and Srebric (2006) measured convective heat transfer on a cooled ceiling in a full-scale laboratory, showing increases of 4–17% when high-aspiration diffusers, installed at the ceiling, supplied 1–5 air changes per hour (ACH). They concluded that air movement enhanced heat transfer not only at the ceiling but also at the walls and floors i.e. not actively cooled surfaces. Other researchers have extended this work to more complex scenarios. Venko et al. (2014) experimentally investigated mixed convection over an active cooling wall with a ceiling slot diffuser. Using derived correlations, they simulated design alternatives in TRNSYS and reported 28–100% reductions in mechanical cooling, depending on air jet velocity, active cooled wall coverage, and internal heat gains. Moftakhari, Bourne, and Novoselac (2023) found that increasing air circulation rates in spaces with radiant panels shifted heat removal from radiative to convective pathways, making loads resemble those of all-air systems. Ventilated slabs, or hollow core slabs, are a related class of TABS in which ventilation air is circulated through embedded ducts within a concrete slab to enhance heat exchange and utilize thermal mass. Thus, the enhanced heat transfer occurs within the concrete slab, not in the occupied space. Studies have shown their potential for peak load reduction, thermal inertia utilization, and advanced control integration under mechanically ventilated conditions (Nevers, Labat, and Malley-Ernewein 2025; Park and Krarti 2019). Airflow rates have been found to be sensitive to the heat transfer rate where the net cooling effect can increase from 2 W m^{-2} at 4 ACH to 8 W m^{-2} at 12 ACH when compared to a conventional HVAC system (Zmeureanu and Fazio 1988). While these studies establish important principles, most predate recent advances in ceiling fan design, control, and comfort standards.

Ceiling fans have recently been re-examined as a practical means of elevated air movement. Karmann et al. (2018) tested ceiling fans integrated with radiant cooled panels in a lab with varying acoustic ceiling coverage. They observed cooling capacity increases of up to 22%, with performance depending on fan direction (i.e. upward, downward, and horizontal). Pantelic et al. (2018) showed that ceiling fans increased slab cooling capacity by ~12% at 24 °C operative temperature and nearly 19% at 26 °C. Guo et al. (2023) quantified convective coefficients under different fan speeds (0.19–0.53 m s^{-1}), reporting an increase of 29–255% compared to no-fan cases. Arumugam, Maiya, and Shiva Nagendra

(2024) experimentally investigated a wall mounted radiant cooling system and reported a 19% increase in cooling capacity as ceiling fan induced air velocity increases from 0 to 0.95 m s^{-1}. Collectively, these findings confirm that elevated air movement consistently enhances radiant system cooling performance, though magnitudes vary with system type, airflow strategy, and boundary conditions.

Beyond system capacity, increased air movement improves occupant thermal comfort. By enhancing convective heat transfer from skin and clothing, ceiling fans enable occupants to maintain comfort at warmer air and mean radiant temperatures (MRT). Tanabe and Kimura (1994) found that participants preferred air speeds of at least 1.0 m s^{-1} at temperatures above 27.8 °C. Similarly, He et al. (2019) reported that occupants adjusted fan speeds (1–1.3 m s^{-1}) to maintain comfort up to 28.9 °C. These experiments indicate a roughly 3 K cooling effect with elevated air movement. Miller et al. (2021) presents a 29-month field study of 99 ceiling fans installed in ten air-conditioned buildings in a hot/dry climate and mean zone indoor temperature increase of 1.9 °C after fan installation, corresponding to mean cooling season compressor energy savings of 36%, normalized by floor area served. More recently, Kent et al. (2023) demonstrated that elevated air movement reduced HVAC energy demand by 32% by allowing 2.5 °C higher indoor setpoints without compromising comfort in an office setting in a hot/humid climate. These results highlight a dual benefit that fans increase radiant system cooling capacity while simultaneously broadening the comfort envelope. However, most of these comfort focused studies evaluate ceiling fans in all-air systems, with limited consideration of their interaction with radiant or TABS configurations.

Despite growing evidence, most prior work at the intersection of air movement and radiant systems has focused on radiant panels or wall systems with diffusers connected to mechanical ventilation systems. The ventilation system replaces zone air, whereas ceiling fans recirculate it. Very limited research directly investigates TABS coupled with ceiling fans, which differ substantially from previous research due to ceiling fan specific airflow patterns, higher thermal inertia, embedded tubing, and broader surface coverage. These characteristics influence surface convection, system capacity, and thermal dynamics which affect occupant thermal comfort. Furthermore, while empirical studies have quantified cooling capacity gains, there is a lack of integration between detailed airflow modelling and whole-building simulation tools, which would enable a systematic exploration of design and operational factors at a low computational cost. This gap has become more pronounced as ceiling fans are increasingly used to support comfort driven and low energy operation in modern buildings.

Accordingly, this study addresses these gaps by investigating the impact of ceiling fan induced air movement on TABS cooling performance using a two-step simulation approach. Through this approach, the study aims to quantify both system-level steady-state cooling heat transfer rate gains and occupant-level comfort improvements from TABS coupled with ceiling fans, offering insights into design strategies that can enhance radiant cooling performance while supporting energy efficiency and comfort goals.

2. Method

In this exploratory study, we investigated how elevated air movement influences the steady-state cooling heat transfer rate of thermally activated building systems (TABS). Although TABS operate dynamically due to their high thermal inertia, designers typically size radiant systems and associated secondary systems based on steady-state capacity. Understanding how ceiling fans modify these steady-state performances is therefore critical for informing design practice.

Our approach involved a sequential modelling approach outlined in Figure 1 with key inputs and outputs from each step in the process. First, we conducted computational fluid dynamics (CFD) simulations in OpenFOAM (Greenshields 2023) to quantify convective surface heat transfer coefficients under varying ceiling fan air turnover rates (ATH), flow directions, and temperature differences between surfaces and room air. We then developed simplified regression models from CFD data for each surface type and airflow direction. In the second step, we integrated these regression models into EnergyPlus (Drury B. Crawley and Lawrie 1999) to simulate whole-building energy performance under different geometric, operational, and design scenarios. By coupling detailed airflow modelling with building simulation, we developed a framework that strikes a balance between accuracy and computational efficiency.

While analytical correlations for convective heat transfer over flat plates provide valuable theoretical insight, they are derived for idealized boundary layer flows that do not reflect the airflow structures generated by ceiling fans. Ceiling fan induced flows are characterized by strong recirculation, flow impingement, and spatially varying turbulence, leading to surface convection mechanisms that differ fundamentally from canonical forced convection (Babich et al. 2017; Chen et al. 2018). The purpose of the CFD analysis is therefore not to revisit established heat transfer theory, but to extend it to a flow regime where analytical similarity solutions do not

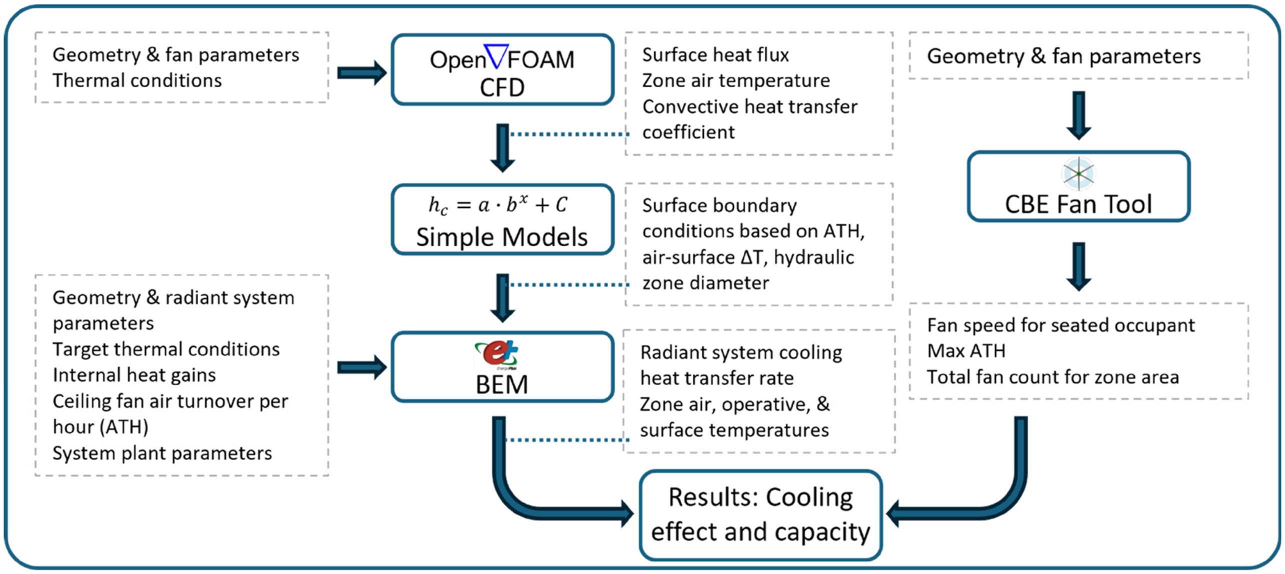

Figure 1. Sequential modelling approach with key inputs and outputs from each step in the process.

exist. This approach enables the development of physically grounded convection models that can be applied within building energy simulation (BEM) tools.

2.1. Convective heat transfer coefficient assessment in OpenFOAM

We modelled airflow and convective heat transfer in OpenFOAM using a representative zone containing ceiling fans and radiant ceiling and floor surfaces. OpenFOAM is an open-source software collection enclosing modules for meshing, solver, and post-processing for CFD analysis. The computational domain was based on a fan cell, occupying one ceiling fan at the centre (see Figure 2). The key dimensions are determined by five geometric parameters: zone width w, zone depth d, zone height h, ceiling-to-fan distance h_f, and fan diameter d_f. Here, we equate w to d, leading to a square floor plan, and set $h = 3.05$ m, $h_f = 0.35$ m, and $d_f = 1.5$ m which are typical values found in commercial office buildings. The fan cell size is determined largely by the zone's overall dimension and the preferred size of the ceiling fan. It is also recommended that the fan diameter be in the range of 0.2–0.4 times the characteristic width of the fan cell to ensure adequate airflow coverage within each cell while minimizing fan-to-fan aerodynamic interference. These fan-related metrics and other layout considerations align with established fan design guidance (Raftery, Fizer, et al. 2019; Raftery and Douglass-Jaimes 2020). Therefore, given a typical fan diameter, we define a 'small' zone made of only one fan cell with zone area $A_{s,zone} = 50$ m^2 ($w = d = 7.07$ m). In order to take into account zone scaling, we consider a second 'large' zone consisting of the 3-by-3 fan cells (i.e. nine equally spaced fans) with $A_{l,zone} = 500$ m^2 ($w = d = 22.36$ m). Zone scaling in this study is based on the total active surface area available for heat exchange, rather than on a strictly geometric replication of fan cells. Radiant system performance and fan induced convective enhancement scale with exposed surface area rather than fan count alone.

The ceiling and floor surfaces represent the radiant system's cooled surfaces, maintained at a constant temperature T_{cc} and T_{cf}, respectively. The four vertical faces of the domain are modelled as solid walls representing adjacent thermal zones or exterior boundary conditions. These faces are assigned a uniform temperature T_h that is necessarily higher than T_{cc} and T_{cf} so as to sustain the desired heat flux direction through the zone. This formulation provides a controlled thermal driving potential across the zone.

We discretized the computational domain using a structured hexahedral mesh with refinement near the walls by using Gmsh's grid distribution algorithm 'bump' to better resolve boundary layer flows (Geuzaine and Remacle 2009, 2022). The near-wall refinement is essential to resolve the steep temperature gradients within the thermal boundary layers to ensure accuracy of the surface heat flux calculations. Using the snappyHexMesh utility in OpenFOAM, we then refine some subcells with the ceiling fan regions in an unstructured manner so that they effectively account for the circular sweeping of the fans. To determine an appropriate grid resolution, we conducted mesh independence tests in the small zone, varying the number of divisions per unit length. We monitored the total steady-state rate of heat flow (W), defined as the

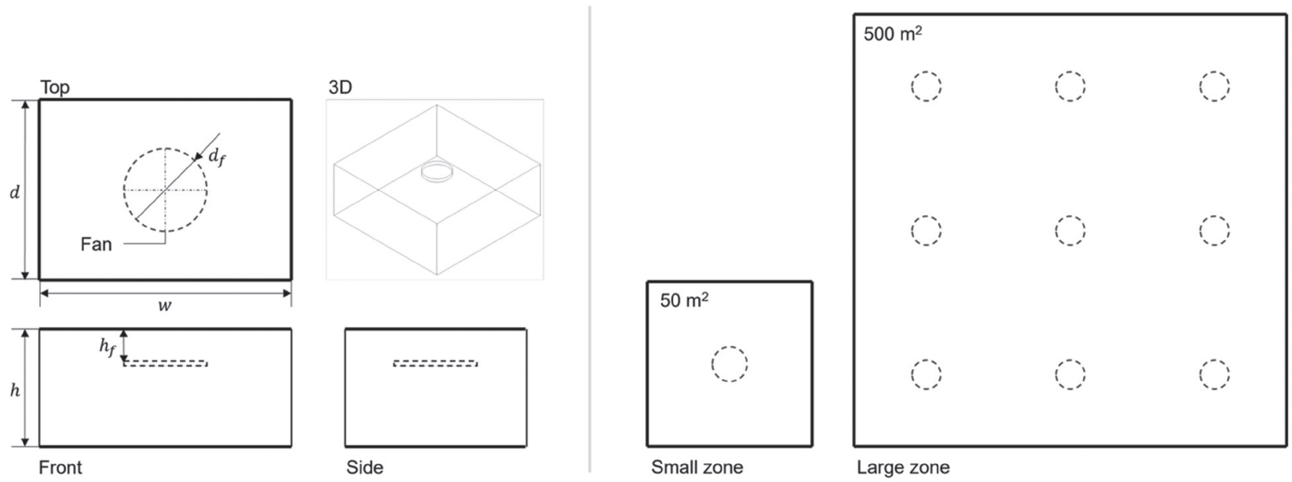

Figure 2. (Left) Schematic of the small square zone with one fan cell and (right) floor plans of small and large zones used to derive surface convective heat transfer coefficients using CFD simulations.

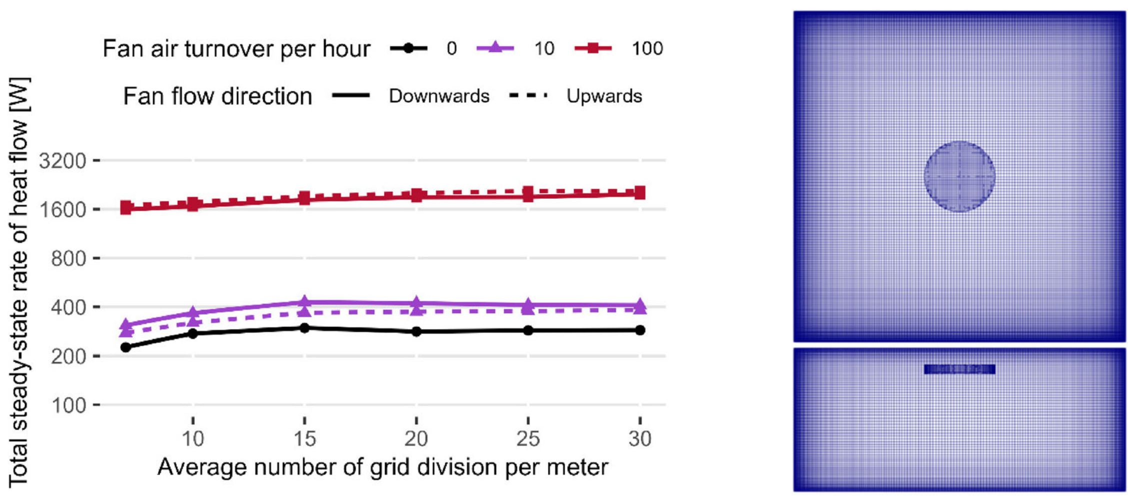

Figure 3. (Left) Mesh dependency test on the case of $T_{cc} = 20\,°C$, $T_{cf} = 20\,°C$, and $T_h = 24\,°C$ with varying air turnover per hour (ATH). Note that the y-axis is on a nonlinear scale and represents the total steady-state rate of heat flow [W] through all cooled surfaces. (Right) Top and front views of the structured hexahedral mesh used for the small zone simulations, also visualizing the central region representing the fan.

area-integrated convective heat flux through all wall surfaces, yielding the comprehensive quantity of the system's heat transfer process. The result given in Figure 3 shows a convergence at 30 divisions per unit length, which we adopted for all simulations. For the small and large zones, the domain is discretized into a total of $212 \times 212 \times 91$ (w x d x h) subcells and $670 \times 670 \times 91$ (w x d x h) subcells, respectively. One may expect to use much finer meshes, but it should be noted that putting more divisions results in an exponential increase in computing resource utilization, while the improvement may be solely tangential. Figure 3 also illustrates the computational grid used in the small zone CFD simulations.

Once the dynamic conditions, including the fan airflow speed v_f and the surface temperatures, i.e. wall T_h, ceiling T_{cc}, and floor T_{cf}, are defined, the programme is ready to solve the flow and temperature fields in the domain. Note that we represent each ceiling fan using a linear momentum source (similar to an actuator disk) rather than resolving blade geometry and rotation. Within the thin cylindrical fan region identified in the mesh (Figure 3), a vertical body force is applied to the fluid to represent the fan thrust. The exact dynamics within and around the fan regions, including complex, blade-dependent vortical flows, may need to be resolved if one wants to acquire accurate outcomes with specific fan models in the whole space. However, our key takeaway from the CFD simulations is the average convective heat transfer coefficients across the entirety of each zone's surfaces, which are distant from the fans. Laboratory experiments and previous CFD analyses suggest this is a valid assumption since researchers found no significant difference in air speeds with various fan models outside the area directly underneath the blades (Chen et al. 2018; Raftery et al. 2019). To streamline the parameters with EnergyPlus, we converted the volumetric airflow rate induced by the fan to air turnovers per hour (ATH), in accordance with Equation 1.

$$ATH = 3600N_f\left(\frac{\pi}{4}\right)d_f^2 v_f/V_{zone} \tag{1}$$

where N_f is the number of fans ($N_f = 1$ for the small zone and $N_f = 9$ for the large zone) and every fan is assumed to operate identically. V_{zone} is the volume of the zone. ATH is a metric used in the ceiling fan industry to distinguish it from ventilation air change rates (ACH) and it takes the meaning of the total volumetric flow rate of air thrusted by the fan(s) per hour, normalized by the zone's volume. Since the airflow field generated by a ceiling fan is inherently spatially non-uniform, the fan speed parameter v_f represents a spatially average vertical over the fan's swept area, used to define the total volumetric flow rate. In the OpenFOAM implementation, this flow rate is used to set the spatially constant thrust (momentum) source term over the fan region. The sign of ATH, which follows that of v_f, may be used to determine the direction of the fan airflow. We treat the upward airflow direction as positive, and vice versa.

In the solver stage, we first used the 'buoyantFoam' application for steady-state flow solutions subject to both thermally driven and fan-induced convections, and then used the 'thermoFoam' application to refine a steady-state zone temperature solution from the previously obtained flow velocity field. For the turbulence closure, we adopted the shear stress transport (SST) k-ω model, a widely used Reynolds-averaged Navier-Stokes (RANS) approach for indoor airflow applications (Menter, Kuntz, and Langtry 2003). The Boussinesq approximation (Zeytounian 2003) serves as the equation of thermal state, where flow incompressibility holds despite the consideration of small linear variations in fluid density with respect to fluid temperature. The approximation remains reasonably accurate for temperature differences up to 28.6 °C, sufficient for typical indoor conditions (Gray and Giorgini 1976). All constant properties of air are taken at 20 °C, at which we also set T_{cc},T_{cf} . We employed the following solution procedure with defined convergence criteria for each stage. First, the buoyantFOAM application was used to compute the airflow field with a target residual threshold of 10^{-3} for all fields. For all cases presented, the velocity field residuals converged below this threshold. As is typical for simulations of turbulent, buoyancy-driven indoor flow, which often exhibit quasi-steady circulations rather than a strictly steady state, the pressure residuals occasionally remained above this threshold when the prescribed iteration limit was reached (5000 iterations for the small zone case and 1500 for the larger zone case, set based on fixed computational time constraints). Under the Boussinesq approximation, the pressure field is not directly coupled to the temperature equation, and convergence of the velocity field is sufficient to ensure convergence of the thermal solution. Then, the converged velocity field was held fixed and supplied to the thermoFOAM application which was run until the temperature field converged with residuals well below 10^{-3}. This procedure ensures that the temperature and heat flux fields used in post-processing are fully converged, stable, and internally consistent. To accelerate convergence, we initialized each case with the solution from the nearest ATH condition with a similar temperature boundary or from the natural convection case (ATH = 0).

After obtaining steady-state solutions given T_{cc}, T_{cf}, T_h, and ATH, we post-processed the results to extract surface heat fluxes ($q_{ceiling}$ at the ceiling, q_{floor} at the floor, and q_{wall} at the sidewalls) and the spatial mean of the zone air temperature T. While local air speeds and convective heat transfer vary with respect to distance from the ceiling fan, extracting the surface-average heat flux inherently integrates these spatial non-uniformities into a single comprehensive metric for the defined fan-cell area. This T is calculated as the volume-average (i.e. bulk) air temperature of the entire zone domain. Finally, we calculated the convective heat transfer coefficients h_c via the following equations:

$$h_{c,ceiling} = \frac{q_{ceiling}}{T_{cc} - T} \tag{2}$$

$$h_{c,floor} = \frac{q_{floor}}{T_{cf} - T} \tag{3}$$

$$h_{c,wall} = \frac{q_{wall}}{T_h - T} \tag{4}$$

Note that $T_{cc,cf} \leq T \leq T_h$. For h_c to be consistently non-negative, we should take the sign of q as positive if heat is transferred into the zone, and vice versa. While T could be defined locally at specific heights within the room (Causone et al. 2009) to evaluate localized draft or comfort, the intended application of the CFD results is their direct implementation into BEM tools (e.g. EnergyPlus) which represent zone air as a single, well-mixed node. Accordingly, we define h_c to relate the integrated surface-specific heat flux to the bulk zone air temperature to ensure consistency with the thermal modelling framework used in BEM tools. We simulated ATH values of 3, 10, 25, 50, and 100 in both the upward and downward fan flow direction plus the natural convection case, i.e. no fan. We evaluate fan flow direction because each will have a distinct airflow pattern in the zone, which will affect the surface integrated convective heat transfer coefficient. We maintained T_{cc} and T_{cf} constant but varied T_h such that the temperature difference between these two surface temperatures varied from 1 to 12 K in 1 K increments for the small zone. For the large zone, we extended this range to 24, 36, 48, and 60 K to capture asymptotic behaviour. We did not model heat transfer by radiation in the zones, as our objective was to isolate convection effects. OpenFOAM model input files are available in the supplementary material.

We compared the CFD results with prior experimental and review studies on radiant surface heat transfer as a consistency check. For natural convection conditions (ATH = 0), Shinoda et al. (2019) provide a comprehensive synthesis of measurements and correlations that we use as a benchmark for baseline convective behaviour. By contrast, few studies examine radiant systems with ceiling fan induced air movement, and even fewer report sufficient detail for direct comparison. Among the available literature Arumugam, Maiya, and Shiva Nagendra (2024) is the only study we identified that experimentally evaluates radiant cooling performance under elevated air movement with ceiling fans with the information required i.e. surface temperatures, air conditions, and heat fluxes.

2.2. Modelling and simulation approach in EnergyPlus

We developed a single zone model with a TABS radiant system in EnergyPlus v8.9 to evaluate the impact of elevated air movement on system performance. EnergyPlus applies the ASHRAE Heat Balance method for zone thermal modelling and has been extensively validated, including against the BESTest standard (Henninger, Witte, and Crawley 2004). It is open-source, publicly available, and capable of simulating radiant system performance (Chantrasrisalai et al. 2003). Since EnergyPlus simplifies radiant piping configurations, we acknowledge that detailed tubing layouts, which can significantly influence heat transfer (Mosa, Labat, and Lorente 2019), are not captured and lie beyond the scope of this study.

2.2.1. Thermal zone and radiant system design parameters

We modelled a single square zone without interior partitions to represent the middle floor of an office building. The zone height was fixed at 3.05 m, with both the floor and ceiling serving as active surfaces for the high thermal mass radiant system. Thus, the floor and ceiling are thermally interconnected. Accordingly, floor and ceiling boundary conditions were set as '*Surface*' while all interior walls were assigned as '*Adiabatic*' conditions. In multi-story buildings employing TABS, a single structural slab is often exposed to the space below as a radiant ceiling and to the space above as a radiant floor. This configuration reflects common construction practice and does not imply identical thermal setpoints or control objectives between adjacent stories. Differences in internal loads and operating requirements are typically addressed through independent control of supply conditions rather than by thermally isolating slab surfaces. Accounting for heat exchange on both sides of the slab, therefore, provides a more realistic representation of radiant system operation.

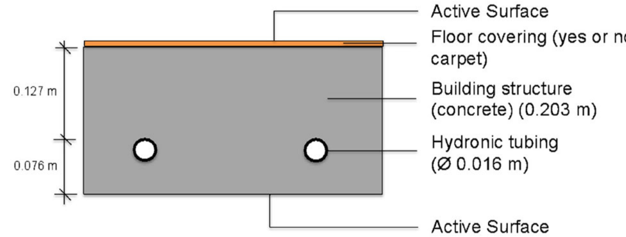

Figure 4. Schematic diagram of the TABS radiant cooling system investigated in this study.

The base-case building has a normal-weight concrete structural slab with embedded hydronic tubing as shown in Figure 4. Tubes with an inside diameter of 0.016 m (5/8 in) were placed 0.127 m below the floor surface, with 0.076 m of concrete below, giving a total slab thickness of 0.203 m. We set tube spacing to 0.152 m and maximum circuit length to 105 m.

The thermal properties of floor/ceiling concrete slab are 1.8 W m^{-1} K^{-1} and 2240 kg m^{-3} for thermal conductivity and density, respectively. We modelled interior walls as medium thermal mass, composed of three layers outside to inside: normal weight concrete (0.1 m thickness, 1.2 W m^{-1} K^{-1} thermal conductivity, 2240 kg m^{-3} density), insulation layer (0.059 m, 0.03 W m^{-1} K^{-1}, and 15 kg m^{-3}), and plasterboard (0.013 m, 0.16 W m^{-1} K^{-1}, 800 kg m^{-3}).

To isolate the impact of air movement on radiant system performance, we held all typically transient schedules constant, including supply water temperature and flow rate within each EnergyPlus simulation. Exterior surfaces and windows were excluded to eliminate solar and diurnal effects. In fixing typically transient disturbances, we effectively represent a 'moment-in-time' snapshot of a specific system's behaviour. While condensation risk is an important design consideration for radiant cooling, we did not explicitly model it. We assumed standard practices apply where the ventilation system maintains indoor humidity such that the zone dewpoint always remains below the lowest supply water temperature, preventing condensation on active surfaces or manifolds. We explored two design supply to return water temperature differences, i.e. 3.3 and 6.7 K, to capture a representative range of design conditions.

2.2.2. Air movement modelling approach

EnergyPlus provides several interior convection models, such as the default model Thermal Analysis Research Program (TARP), Simple, Adaptive, and Ceiling Diffuser, along with case-specific equations. However, no universally accepted 'best model' exists for interior convective heat transfer, and critically, EnergyPlus lacks a model to represent ceiling fan induced air movement. To address this gap, we developed six regression-based models using the CFD results described in section 2.1. Each model accounts for surface type (floor, ceiling, or wall) and fan flow direction (upward or downward). We considered a regression model with three independent variables of the form shown in equation 5.

$$h_c = A \times ATH^{\alpha} + B \times \Delta T^{\beta} + G \times {D_h}^{\gamma} + C \qquad (5)$$

where $A, B, G, C, \alpha, \beta$, and γ are model parameters derived from CFD data, ATH [-/h] is the fan air turnover rate, ΔT [K] is the temperature difference between mean zone air and surface temperature, and D_h [m] is the hydraulic diameter of the zone calculated as four times the zone area divided by its perimeter. Prior studies on radiant systems with mechanical ventilation (Jeong and Mumma 2003; Novoselac, Burley, and Srebric 2006) have employed mixed-convection correlations that express the convective heat transfer coefficient as a combination of airflow-related and temperature-difference terms. In some situations, they account for zone scale geometry. Thus, we took a similar approach, but we are using ATH instead of diffuser air velocity or ACH.

We implemented these models in EnergyPlus using '*EnergyManagementSystem*' (EMS) objects. At each timestep, the EMS program recalculates h_c for ceiling, floor, and wall surfaces based on ΔT, overriding the default convection coefficients. While ATH and flow direction remain fixed within a given model run, ΔT is updated dynamically as the simulation approaches steady state. This framework offers a practical approach to representing ceiling fan effects in whole-building simulations. The same approach can be easily extended to dynamically vary ATH based on a schedule or in response to other dynamic simulation variables, enabling the evaluation of integrated radiant and ceiling fan operation for occupant comfort, energy efficiency, and grid-responsive control in annual simulations. An example EnergyPlus model idf that includes the EMS program to override the convective heat transfer coefficient is available in the supplementary material.

Table 1. Summary of design parameters and their levels to create 3,536 valid models with unique combinations.

Design Parameters	Levels
Air turnover per hour (ATH)	0 (natural convection), 3, 10, 20, 30, 60, 100
Zone floor area [m^2]	50, 100, 200, 500
Fan flow direction	Downwards, Upwards
Radiant system supply water temperature [°C]	15, 18, 21
Radiant system tube spacing	0.1524 m (6 in), 2286 m (9 in)
Floor Covering (carpet)	No, Yes (R-value $= 0.335\ m^2\ K\ W^{-1}$)
Target/Baseline zone operative temperature [°C]	24, 26, 28
Target/Baseline supply-return water temperature difference [°C]	3.3, 6.7

2.2.3. Design factors evaluated

We evaluated geometric, operational, and design factors to characterize the performance of the TABS and ceiling fan coupled system. As a source of variation to evaluate the influence of wall heat transfer on the results, we adjusted the floor area of the zone using four levels (see Table 1). In larger zones, walls have much less effect on surface heat transfer than in smaller zones. We vary the following design parameters: fan ATH (i.e. the combination of different surface convection coefficient values for ceiling, floor, and walls), fan flow direction, radiant system supply water temperature, radiant system tube spacing, and the existence of a carpet layer. We obtain an initial model list by performing a full factorial design on the design parameters and levels in Table 1. The selected design parameters are within the recommendations and constraints of established standards (ASHRAE 2023; ISO 2021), design guidelines (Babiak, Olesen, and Petras 2009), previous research (Duarte Roa et al. 2025), and exemplary manufacturer specifications (Uponor 2013).

This results in a list of 4,032 models. However, we post-process the initial full-factorial set to adjust the target zone operative temperature since it is possible to combine the target zone operative temperature, radiant supply water temperature, and supply-return temperature difference in unrealistic scenarios. Thus, when the sum of the radiant supply water temperature and supply-return temperature difference was greater than the target zone temperature, we added 2 K to the sum of the radiant supply water temperature and supply-return temperature difference and rounded up to the next whole value to obtain the new target zone operative temperature. We remove 224 duplicates from this post-process step. We also remove 272 duplicate natural ventilation cases that result from combining zero ATH cases with the downward and upward parameters which are irrelevant for that scenario. In total, we evaluated 3,536 unique combinations of the design parameters.

Then, we present two scenarios. In the first scenario, referred to as Scenario 1, we aim to maintain a target zone operative temperature (±0.25 °C) and a target supply to return water temperature difference (±0.1 K) as we vary the design parameters mentioned above. Achieving these conditions requires an iterative adjustment of internal heat gains and radiant system water flow rate. Scenario 1 allowed us to isolate the effect of ceiling fans on radiant system steady-state cooling heat transfer rate while holding operative conditions constant. In the second scenario, referred to as Scenario 2, we initiate with 272 baseline models from Scenario 1 in which no fans were modelled. These baseline models already achieved the target operative temperature and supply-return water temperature difference using the internal heat gains and radiant system water flow rate found in Scenario 1. We then varied ATH and air flow direction, but unlike Scenario 1, we did not adjust heat gains or water flow rates, as compared to their respective no-fan baseline (ATH = 0). As a result, the steady-state operative temperature and supply-return water temperature difference were different for models with higher air movement when compared to their no-fan baseline. Scenario 2, therefore, captures the effect of fans on zone thermal conditions under steady-state system operation.

Scenarios 1 and 2 are intentionally structured to decouple system-level steady-state cooling heat transfer rate enhancement from occupant-level comfort enhancement. In practice, the combined effect would arise under fan-assisted operation control strategies in which increased air movement simultaneously enhances radiant system performance and occupant heat transfer, without imposing artificial constraints, to respond to varying weather conditions and internal load disturbances. Together, the two scenarios enable us to evaluate three outcomes: (1) increases in radiant system steady-state cooling heat transfer rate at constant zone operative temperature T_{op}; (2) changes in operative temperature, reference temperature difference ΔT_h, and equivalent heat transfer coefficient K_H at fixed load; and (3) the cooling effect of air movement, expressed as an equivalent temperature reduction experienced by occupants. The reference temperature difference (ΔT_h) [K] and equivalent heat transfer coefficient (K_H) [W m^{-2} K^{-1}] are presented in equation 6 and equation 7, respectively (ISO 2021).

$$\varDelta T_h = \frac{T_{wo} - T_{wi}}{ln[(T_{wi} - T_{op})/(T_{wo} - T_{op})]} \tag{6}$$

$$K_H = \frac{q}{\varDelta T_h} \tag{7}$$

where, T_{wi}, T_{wo} [°C] are the supply and return water temperature, respectively, T_{op} [°C] is the zone operative temperature, and q is the surface heat flux for the active surface.

We use equation 8 to calculate the cooling effect for the various EnergyPlus models we simulated. Equation 8 uses the standard effective temperature (SET) which is a thermal comfort index defined and used by ASHRAE Standard 55 to assess the cooling effect of air movement into an equivalent temperature. SET represents the temperature of an imaginary, uniform environment where an imaginary occupant with standard activity and clothing levels would experience the same total heat loss from the skin as the actual person in the actual, non-uniform environment. SET is computed using a human thermoregulation model and explicitly integrates the combined effects of air temperature, MRT, humidity, air movement, clothing insulation, and metabolic rate. Unlike air temperature alone, SET accounts for both convective and radiative heat exchange between the occupant and the surrounding environment. Importantly, SET also captures the influence of elevated air movement, which increases convective and evaporative heat loss and can substantially reduce perceived warmth without changes in air or surface temperature, i.e. cooling effect. Therefore, SET is an appropriate metric for comparing thermal comfort across different combinations of radiant operating conditions and air speeds. Luo et al. (2021) also used this calculation to similarly evaluate the cooling effect of air movement in non-radiant system building spaces. We used the CBE Fan Tool (Raftery 2019) to determine the fan cell size for a typical office fan installation for each zone size we simulate and models outlined in Raftery et al. (2019) to estimate the air speeds for seated occupants. We selected a fan type from the tool that can achieve at least 100 ATH. We assumed standard office occupants working in summer (e.g. 50% RH, 1.1 MET, and 0.5 CLO). We obtained zone air and mean radiant temperatures from the EnergyPlus simulations.

$$CoolingEffect = SET_{stillair} - SET_{airmovement} \tag{8}$$

3. Results

We first present CFD flow field visualization to illustrate the airflow mechanisms through which ceiling fans

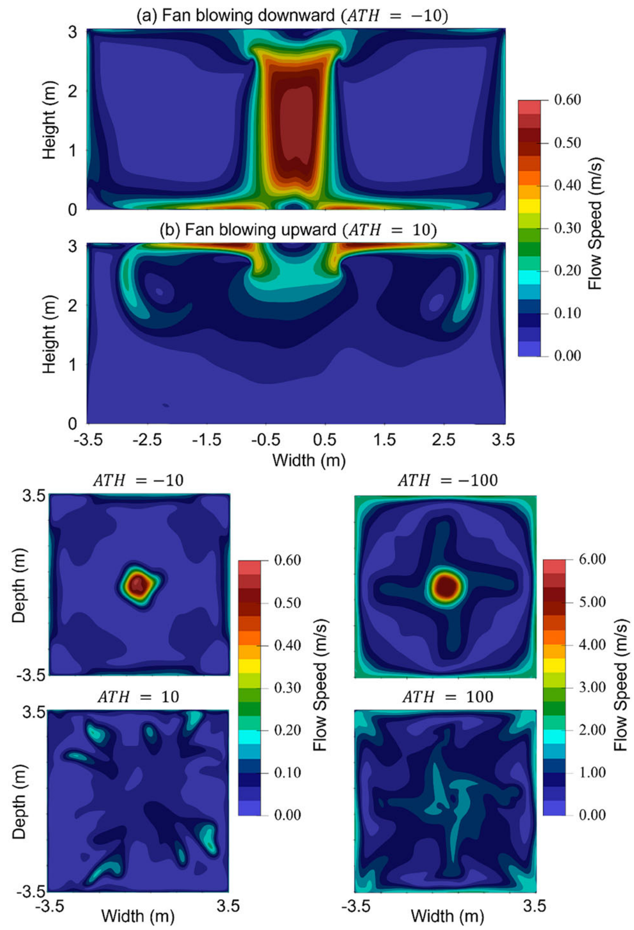

Figure 5. (Top) Cross-sectional velocity magnitude contours ($x = 0$ plane) comparing downward fan flow (ATH $= -10$) and upward fan flow (ATH $= 10$). (Bottom) Velocity magnitude contours at occupant height (z $= 1.1$ m) comparing downward (ATH $= -10, -100$) and upward (ATH $= 10, 100$) flow directions. Data for both figures taken from the cases at T_{cc},T_{cf} $= 20$ and $T_h = 26$ °C.

enhance radiant system heat transfer rate. Figure 5 (top) shows the velocity field for downward and upward fan operation at the same airflow magnitude (ATH $= 10$), highlighting the distinct flow structures generated by each configuration. In the downward case, a high momentum jet impinges on the floor, strongly enhancing near floor mixing and convective heat transfer. Conversely, upward operation directs airflow toward the ceiling where it spreads radially and promotes enhanced convection across the ceiling surface. In both cases, the resulting increase in overall room scale mixing improves convective heat transfer at the opposing surface and increases the total heat flux. Figure 5 (bottom) further illustrates the spatial distribution of air speed at the occupied level, demonstrating the inherent non-uniformity of fan induced flows and the contrasting comfort implications of upward versus downward operation. Upward airflow may be a superior choice for avoiding local discomfort since it produces more diffused, uniform airflow. The concentrated high velocity jets from a downward airflow may increase draft risk for occupants seated directly below. These flow visualizations provide physical context for the surface-averaged convective heat transfer coefficients and system-level performance trends discussed in subsequent sections.

Similarly, the thermal mechanism by which ceiling fans enhance convective heat flux is illustrated in Figure 6, which compares the temperature field under natural convection with fan-induced airflow at 25 ATH. Under natural convection, the zone exhibits pronounced thermal stratification, with warm air accumulating near the ceiling and thick thermal boundary layers forming along the enclosure surfaces, particularly in the sidewall-ceiling corners. This stable stratification causes warm and cool air to remain adjacent to the respective hot and cooled surfaces, effectively increasing thermal resistance and limiting heat transfer. In contrast, fan-assisted convection fundamentally alters the zone's thermal structure by generating a well-mixed core with more uniform temperature distribution. Fan-driven circulation compresses the thermal boundary layers against the active surfaces, thereby reducing convective resistance. The conceptual streamlines further illustrate how the fan induced flow (blue arrows) entrains bulk air and drives it along the walls and floor, overcoming buoyancy-driven circulation (red arrows) that otherwise sustains stratification. This disruption of the buoyancy-dominated flow regime reduces the overall thermal resistance of the zone and enables higher convective heat transfer rates.

3.1. *Convective surface heat transfer coefficients from CFD*

Figure 7 and Figure 8 present the effects of ceiling fan induced air movement on convective surface heat transfer coefficients and heat fluxes in the large zone. Results are plotted as functions of the temperature difference between mean zone air and the cooled surface temperature (ΔT), for a range of ATH, flow directions, and surface types. For the no-fan baseline condition (ATH $= 0$), we include established natural convection correlations from the literature, summarized by Shinoda et al. (2019) and current ASHRAE guidance, solely for reference and validation of the natural convection regime. The CFD results for this baseline align closely with ASHRAE guidance, while greater variability is observed among other experimental correlations reported in the literature, particularly for floor and wall surface coefficients. For fan driven cases (ATH > 0), comparable reference correlations are largely unavailable. Instead, we plot the results of the simplified regression models developed in this study (equation 5

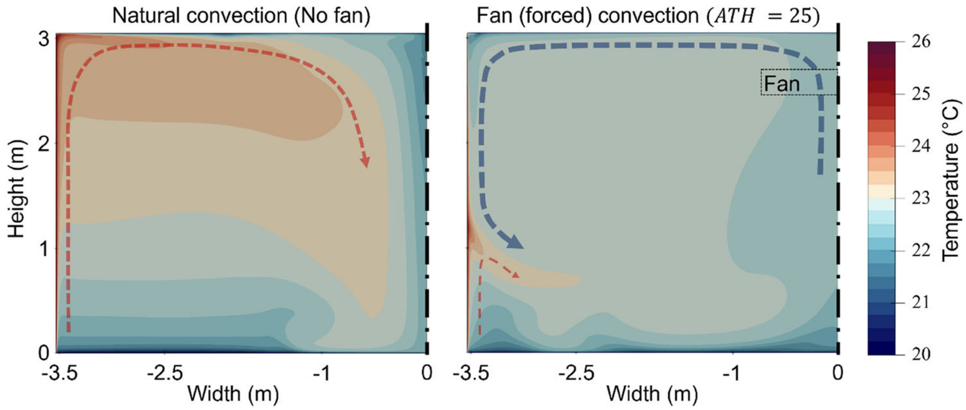

Figure 6. Temperature contours with conceptual flow streamlines at the $x = 0$ plane comparing (left) natural convection and (right) forced convection at ceiling fan ATH = 25. Fan induced flow (blue arrows) entrains bulk air and drives it along the walls and floor, overcoming buoyancy-driven circulation (red arrows) that otherwise sustains stratification. Data for both figures taken from the cases at T_{cc},T_{cf} = 20 and T_h = 26 °C.

and Table 3), shown as black 'x' symbols and labeled 'Simple Model', which demonstrates close agreement with the CFD data. Arumugam, Maiya, and Shiva Nagendra (2024) experimentally evaluated wall-mounted radiant panels under ceiling fan operation for ATH values up to 86. However, their reported convective coefficients differ from the present Simple Model results by 27–50%. Notably, substantial variability was also observed in their natural convection measurements, which limits direct comparison. We found similar trends in the small zone (see Supplementary material A1). Readers can also refer to the supplementary material for high-level results for the CFD simulations.

As expected, convective heat transfer coefficients increased with higher ATH, confirming the positive relationship between air movement and surface convection. With respect to temperature difference, the coefficient values rose sharply between 0 and 3 K, then plateaued as values stabilized. This indicates that momentum-driven effects due to fan operation, rather than buoyancy driven effects due to the surface to air temperature gradient, are the dominant driver of increased convection. Effects at very low fan speeds ($\leq$ 3 ATH) were negligible, particularly in the small zone, suggesting that significant increase in convective heat transfer requires higher airflow rates. Table 2 summarizes the average percentage change in convective coefficients for $\Delta T > 3$ K compared to natural convection (ATH = 0). Both small and large zones required ATH $>$ 3 for measurable increases. Flow direction also played a role. That is, a downward flow produced larger gains at the floor surface while an upward flow more strongly affected the ceiling. Effects on walls were modest but became more noticeable in larger zones and at high ATH. The strongest relative increases were observed at the floor, where natural convection is weakest. Without fans, cool dense air tends to stagnate near the floor, suppressing convection. Fan induced air movement disrupts this stratification, substantially increasing forced convection and heat transfer.

Table 3 reports regression parameters for six simplified convection models based on the form shown in equation 5, each representing a surface type and fan flow direction. These models are valid for ATH $\geq$ 10, as coefficients at lower fan speeds resemble no-fan cases. The regression model estimations were also plotted in Figure 7 and Figure 8 (black 'x'), showing close agreement with CFD data. In addition, selected simple regression model estimates are presented in table form in the appendix for the large zone. Goodness of fit statistic confirms this with R^2 values exceeding 0.96, root mean square error (RMSE) ranging from 0.36 to 0.72, and mean absolute percentage error (MAPE) ranging from 3.7 to 14.1%. Higher MAPE values were associated with upward flow at the floor, reflecting greater variability in these conditions. Overall, the CFD analysis demonstrates that ceiling fans significantly enhance convective heat transfer coefficients, particularly at higher ATH and for floor surfaces prone to air stagnation. We implemented these models in EnergyPlus to evaluate system-level impacts of TABS and ceiling fan coupled systems under a wide range of design and operational scenarios as detailed in section 2.2.3.

3.2. *Heat transfer rate and temperature results from EnergyPlus*

Table 4 summarizes inputs and outputs from the CBE Fan Tool, and Figure 9 shows the estimated occupant-level air speeds for various ceiling fan ATH values and zone areas. We used these air speeds to estimate the

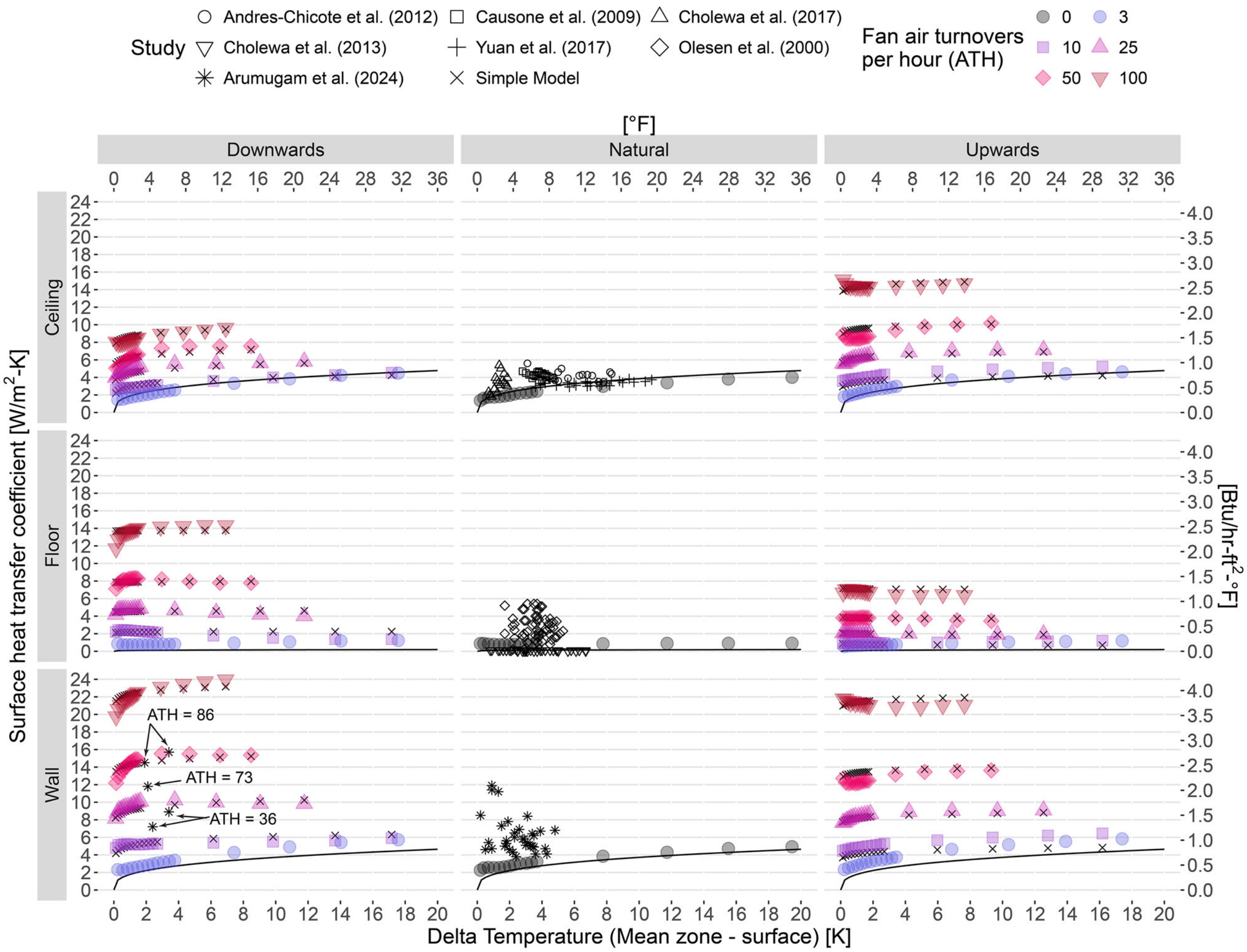

Figure 7. Ceiling, floor, and wall convective surface heat transfer coefficient of a large zone (500 m^2) for various ceiling fan air turnover per hour (ATH), fan flow direction, and temperature difference between the mean zone air and zone surface. The colored shapes indicate CFD derived points, and the black outlined shapes indicate references found in the literature (Shinoda et al. 2019). Natural refers to the no-fan condition and the solid black line refers to the ASHRAE references with no fans. Simple model predictions calculated from equation 5 using parameters in Table 3 are shown with black 'x'.

Table 2. Average percentage change in convective surface heat transfer coefficient at 3 K and above temperature difference between mean zone air and surface temperature from zero air turnovers per hour (ATH) reference. The calculations are performed from the CFD data. Values on the left of the '|' are for the small zone and values on the right are for the large zone.

Surface	Fan flow direction	ATH 0	3	10	25	50	100
floor	downward	–	−12% | 14%	150% | 79%	504% | 405%	862% | 818%	1570% | 1572%
ceiling	downward	–	3% | 10%	1% | 35%	42% | 87%	88% | 149%	201% | 211%
wall	downward	–	0% | 11%	36% | 44%	148% | 157%	266% | 296%	515% | 510%
floor	upward	–	−8% | 13%	20% | 28%	185% | 130%	505% | 322%	855% | 651%
ceiling	upward	–	4% | 25%	30% | 64%	104% | 132%	208% | 224%	431% | 379%
wall	upward	–	1% | 22%	28% | 56%	123% | 132%	276% | 246%	528% | 439%

cooling effect in Scenarios 1 and 2 as described below. As noted by Raftery et al. (2019), the airflow models apply to downward fan operation. Reversing fan direction at the same rotational speed typically produces lower but more uniform air speeds. For the fan sizes modelled here, rated airflow was sufficient to exceed the maximum simulated value of 100 ATH in the downward direction. The extra capacity may be enough to achieve comparable air speeds for the upward airflow. For each zone, we calculated minimum, maximum, and area-weighted mean air speeds. Minimum values occur at fan cell edges, maximum under the blades, and area-weighted averages reflect typical seated occupant exposure.

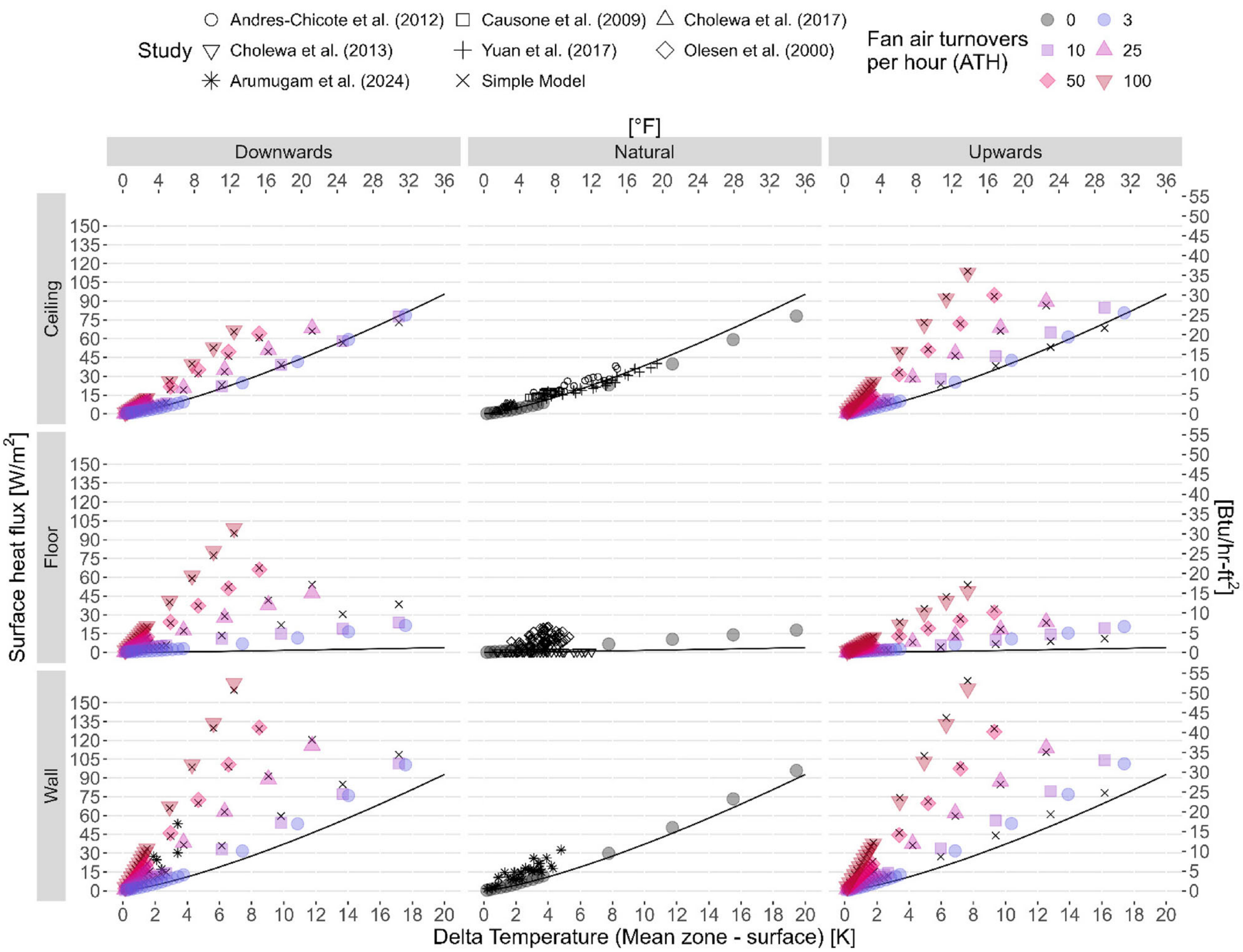

Figure 8. Ceiling, floor, and wall surface heat flux of a large zone (500 m^2) for various ceiling fan air turnover per hour (ATH), fan flow direction, and temperature difference between the mean zone air and zone surface. The colored shapes indicate CFD derived points, and the black outlined shapes indicate references found in the literature (Shinoda et al. 2019). Natural refers to the no-fan condition and the solid black line marks the ASHRAE references with no fans. Simple model predictions calculated from equation 5 using parameters in Table 3 are shown with black 'x'.

Table 3. Convective surface heat transfer coefficient model parameters derived from the CFD simulation test cases for various surface types and fan flow directions. The last three columns show the coefficient of determination (R^2), root mean square error (RMSE), and mean absolute percentage error (MAPE) to indicate the simple models' goodness of fit.

Surface	Fan flow direction	A	α	B	β	G	γ	C	R^2	RMSE	MAPE
floor	downward	0.36	0.7944	−0.79	−0.034	4.63	−0.0825	−2.84	0.993	0.361	6.2%
ceiling	downward	0.93	0.4794	4.43	0.0894	2.67	0.1759	−8.89	0.969	0.382	5.8%
wall	downward	1.18	0.64	11.59	0.0367	7.15	0.0524	−20.10	0.993	0.542	3.7%
floor	upward	0.13	0.8706	9.91	−0.0036	6.71	−0.1783	−13.97	0.978	0.360	14.1%
ceiling	upward	1.08	0.5696	5.54	0.0473	3.12	0.0641	−9.90	0.977	0.620	7.1%
wall	upward	1.12	0.6492	6.68	0.0344	83.30	−0.0064	−89.17	0.988	0.718	6.1%

Table 4. Relevant inputs and outputs of the CBE Fan Tool to estimate the air speeds for a seated occupant for ceiling fan(s) with downward flow.

Zone area [m^2]	Fan cell size (w x d [m])	Fan diameter [m]	No. of fans in zone	Max fan air speed [m/s]	Rated fan airflow [m^3/s]	Max zone ATH
50	7.07 × 7.07	2.1	1	2.16	7.73	183
100	5 × 5	1.5	4	2.1	3.83	181
200	7.07 × 7.07	2.1	4	2.16	7.73	183
500	7.45 × 7.45	2.1	9	2.16	7.73	164

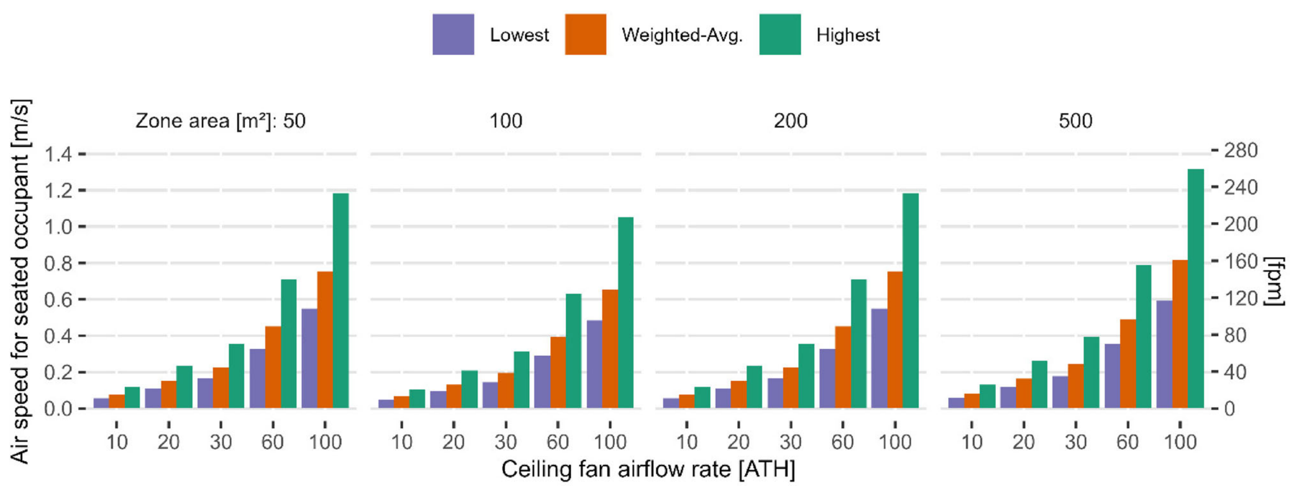

Figure 9. Estimated air speeds for a seated occupant for various ceiling fan air turnovers per hour (ATH) and zone floor areas. The air speeds are based on models developed in (Raftery, Fizer, et al. 2019) for downward flow. The 'Lowest' and 'Highest' values represent the model predictions for the lowest and highest air speeds in a space with a specified fan, and the 'Weighted-Avg.' represents the room area weighted average air speed in the space.

3.2.1. *Scenario 1: targeted operation temperatures*

In Scenario 1, we vary the internal heat gains and radiant water flow rates to maintain both a target operative and a fixed supply to return water temperature difference. Figure 10 shows a limited set of data from EnergyPlus simulations to better illustrate the impact of the target zone operative temperature, temperature difference between zone operative and active radiant surface temperature, and ceiling fan airflow rate on the steady-state cooling heat transfer rate (radiant plus convective) of the radiant system. We evaluate steady-state cooling heat transfer rate as a function of the temperature difference between the zone operative and active surface temperature, rather than air-surface temperature difference. Operative temperature captures the combined effects of air temperature and MRT and therefore represents the relevant thermodynamic driving potential for total heat exchange in radiant systems. Using operative temperature also allows us to compare the steady-state cooling heat transfer rate under equivalent physical thermal conditions. However, they are not the same perceived occupant thermal comfort conditions since air movement induces a cooling effect on occupants as shown below.

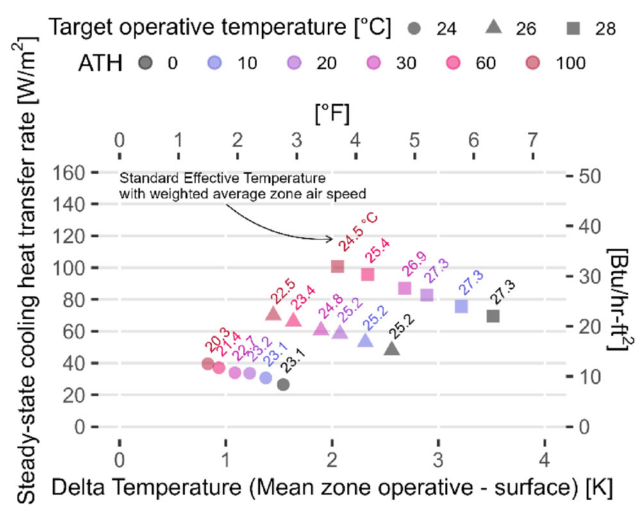

Figure 10. Three model groupings to illustrate the impact of the temperature difference between zone operative and active radiant surface temperature, target zone operative temperature, and increased ceiling fan air turnover per hour (ATH) on steady-state cooling heat transfer rate. Each model has its resulting Standard Effective Temperature annotated. The three model groupings have the following same parameters: fan flow direction = downwards, zone floor area = 100 m^2, floor covering = none, radiant system supply water temperature = 18 °C, target supply-return water temperature difference = 3.3 °C, and radiant system tube spacing = 0.1524 m.

Figure 10 presents three model groupings, each with a target zone operative temperature of 24, 26, or 28 °C. Each model within the group, represented by color, shows the impact of various ATH. As mentioned above, an ATH of 3 results in a similar performance as the no-fan case and we excluded it from further analysis. The rest of the design parameters in Table 1 remain at the same level for all models in Figure 10. Figure 10 shows that the steady-state cooling heat transfer rate increases with higher target zone operative temperature because the operative to surface temperature difference widens. Both air and radiant surface temperatures rose, though air temperature increased more rapidly, producing greater cooling heat transfer rate. Fan operation further boosted cooling heat transfer rate while reducing the operative to surface temperature difference. Although the zone operative temperature remains the same among each group defined

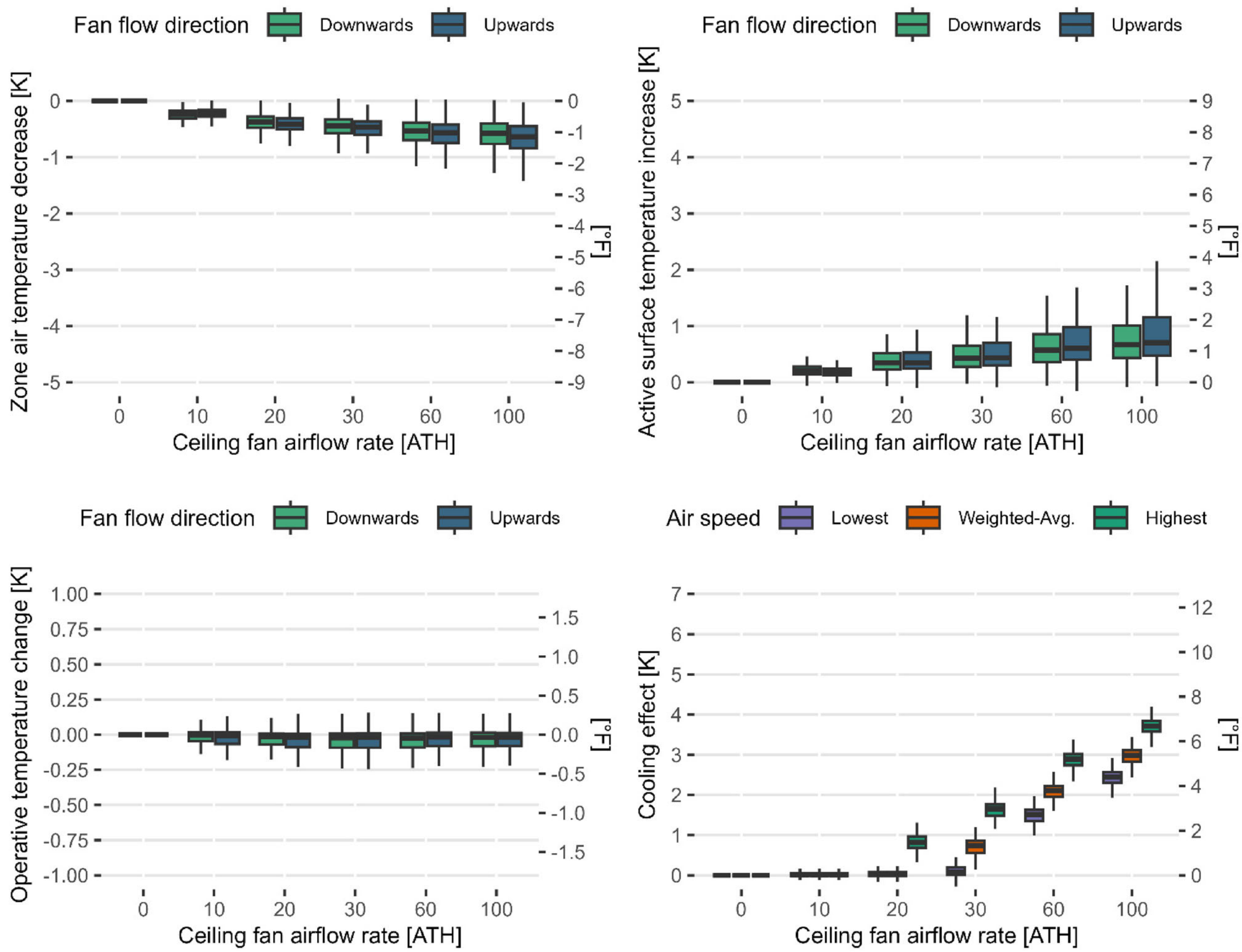

Figure 11. The impact on (top-left) zone air, (top-right) active surface, and (bottom-left) operative temperatures when maintaining a constant design zone operative temperature and supply to return water temperature difference as ceiling fan air turnover per hour (ATH) increases for Scenario 1. These combined dynamics result in a (bottom-right) cooling effect due to air movement.

by shapes in Figure 10. There are a couple of dynamics occurring that result in a lower temperature difference as ceiling fan ATH increases. First, the increase in cooling heat transfer rate from elevated air movement results in warmer radiant surface temperatures. Second, the zone air temperature decreases compared to the no-fan case and approaches the target operative temperature with increasing air movement. Figure 11 shows these effects on aggregate from all the simulations in Scenario 1. Both effects result in lower temperature differences between zone operative and active radiant surface temperatures. The temperature changes are more pronounced for zones with higher zone operative temperatures. That is, the drop in the temperature difference between zone operative and active radiant surface temperature is 1.46 K from 0 to 100 ATH at 28 °C versus only 0.71 K for the 24 °C case. This is also shown visually in Figure 10 through the spread of the results within each model group. Lastly, as air movement increases within the zone, the Standard Effective Temperature decreases, producing a measurable cooling effect at higher ATH levels. For example, comparable thermal comfort can be achieved at an operative temperature of 28 °C with ATH = 100 as at 24 °C with ATH = 0. Figure 11 shows the aggregate cooling effect of increasing ceiling fan ATH while maintaining constant zone operative temperatures. The cooling effect can reach a median of up to 3.71 K for the highest air speeds.

Figure 12 shows all the data for Scenario 1, and it shows the same relationships described above for Figure 10. Figure 12 also shows that the operative to active surface temperature difference is about 5 K in the models simulated under steady-state conditions. Furthermore, it shows a maximum cooling heat transfer rate of 150 W m^{-2} with elevated air movement, which is noteworthy since radiant systems are often cited as having limited cooling capacity under current standard design practices,

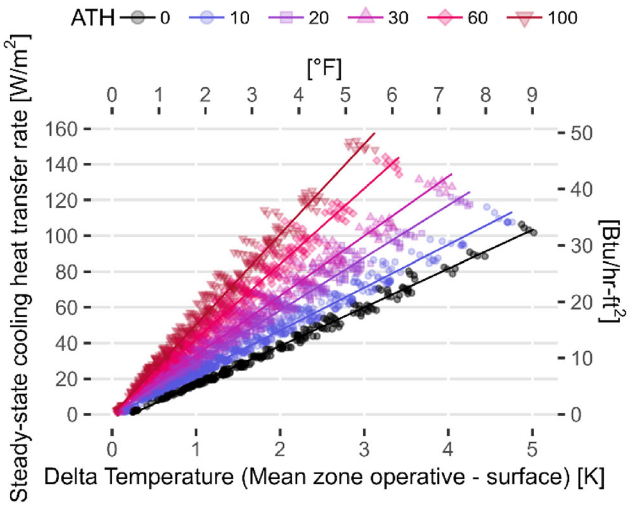

Figure 12. Steady-state cooling heat transfer rate as a function of the temperature difference between zone operative and active radiant surface temperature, grouped by ceiling fan air turnover per hour (ATH). Each group has a linear regression trend superimposed.

e.g. a peak surface heat extraction rate of about 31 W m^{-2} (Duarte Roa et al. 2025).

Figure 13 quantifies the incremental cooling heat transfer rate from elevated air movement relative to no-fan baselines. Median increases rose from 3.0 (IQR: 1.6–4.4) W m^{-2} at 10 ATH up to 13.5 (8.4–21.7) W m^{-2} at 100 ATH under upward flow, with a maximum absolute increase of 48.7 W m^{-2}. Normalized to baseline capacities, these represent gains of 9.5% (6.3–13.3%) at 10 ATH and up to 47% (42.6–53.0%) at 100 ATH. Furthermore, the models' total cooling heat transfer rate starts diverging between the downward and upward airflow direction groups at 20 ATH, reaching an 8% median difference at 100 ATH, with upwards airflow yielding higher cooling heat transfer rates at the same fan airflow rate.

Reference temperature difference remained stable for models sharing the same target operative temperature and supply to return water temperature difference across different ATH, flow directions, pipe spacing, floor covering, and floor area (see Supplementary material B1). However, in general, it decreases as zone operative temperature decreases, supply water temperature increases, or as the supply to return water temperature difference increases. Equivalent heat transfer coefficient showed clearer sensitivity where values increased with lower supply water temperature, higher ATH, higher operative temperature, tighter pipe spacing, smaller supply to return water temperature difference, and absence of carpet (See Figure 14). Zone size and fan airflow direction have little effect on the overall equivalent heat transfer coefficient.

3.2.2. Scenario 2: fixed total design cooling capacity

Scenario 2 began with the 272 baseline models from Scenario 1 that achieved the target operative temperature and supply to return temperature difference without fans. We fixed the internal heat gains and radiant system water flow rate and varied fan ATH and flow direction. As a result, cooling capacity was fixed and only zone temperatures varied. Figure 15 shows that increasing ATH lowered both air and non-active surface temperatures, while active surface temperatures remained nearly constant due to the fixed waterside inputs. Compared to the natural convection case, air temperatures fell by 0.57 K (0.45–0.73) at 10 ATH to 1.58 K (1.15–2.46) at 100 ATH. Non-active surfaces cooled by 0.16 K (0.10–0.23) at 10 ATH to 1.01 K (0.71–1.74) at 100 ATH. The overall effect

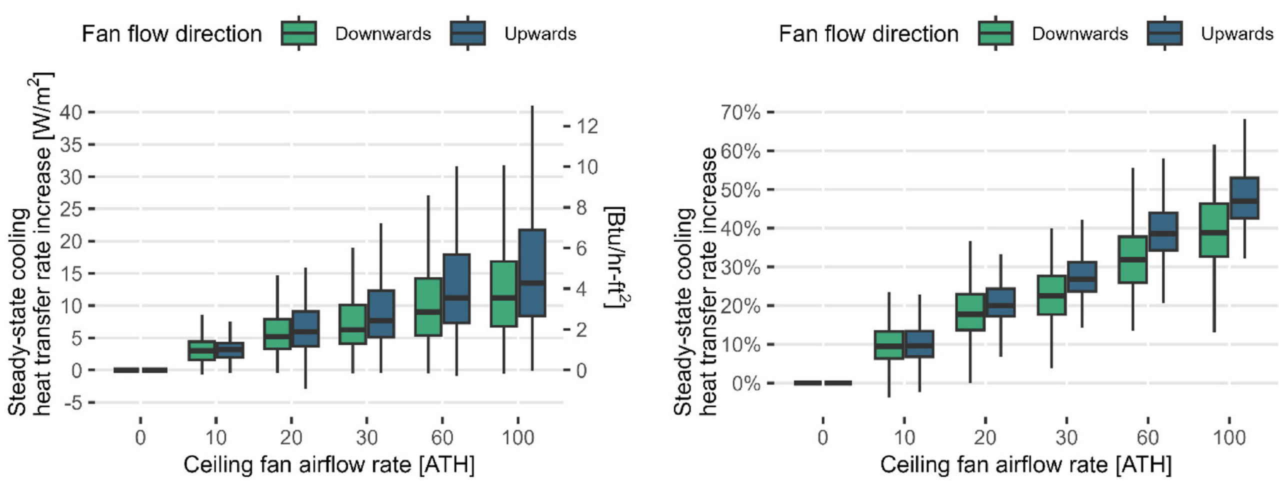

Figure 13. Steady-state cooling heat transfer rate increase as a function of ceiling fan air turnover per hour (ATH) grouped by airflow direction represented as (right) absolute cooling load per square meter increase from their respective baseline, e.g. the no-fan case and (left) normalized as a percentage increase from their respective baseline.

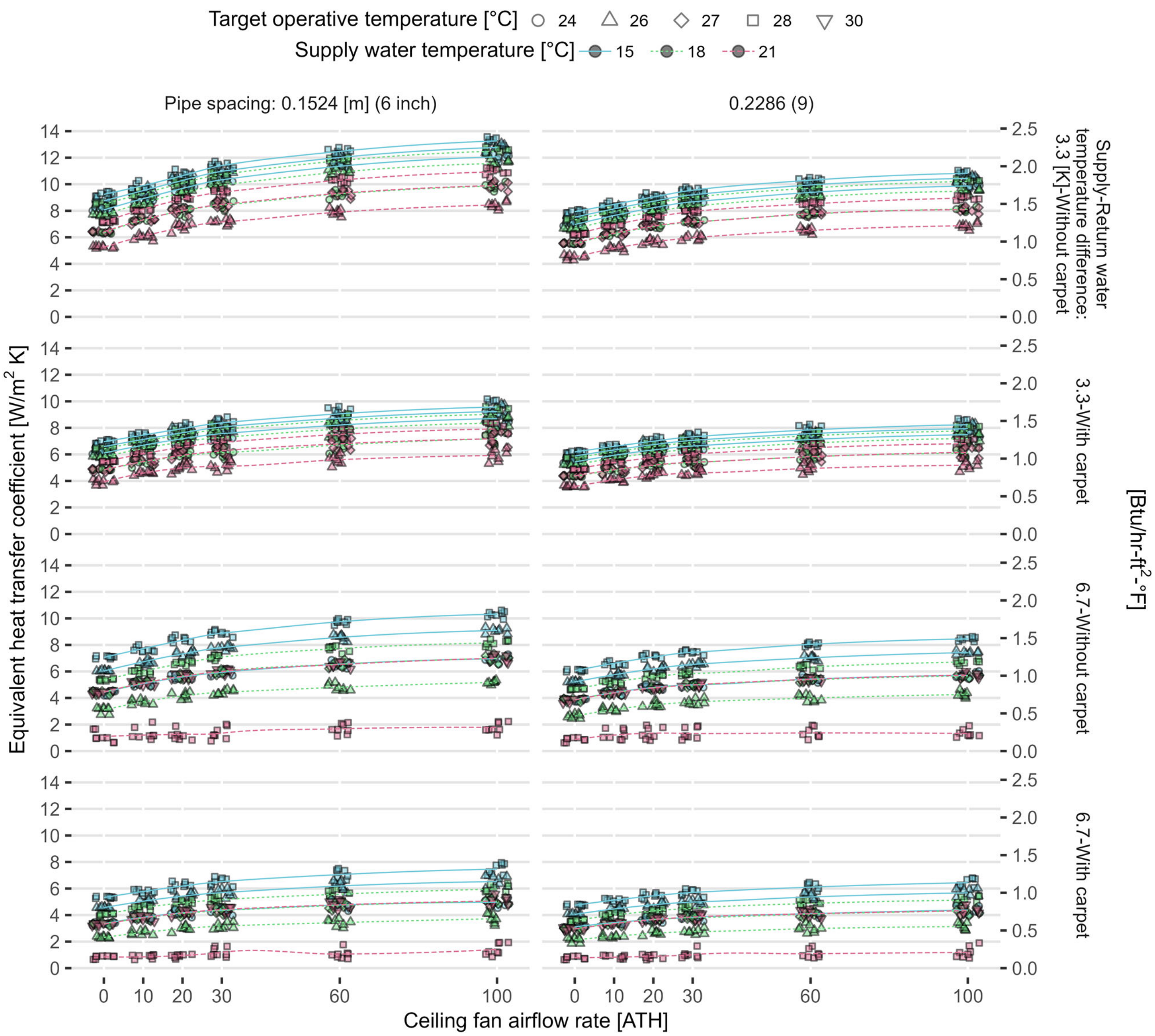

Figure 14. The effect of various design parameters on equivalent heat transfer coefficient (K_H) when we vary the internal heat gains and the radiant system water flow rate to achieve a target zone operative temperature and supply to return water temperature difference as we vary the ceiling fan air turnover per hour (ATH). Point jitter is added to the x-direction to help visualize the type and density of points at each ATH.

causes the operative temperature to drop from 0.33 K (0.26–0.44) at 10 ATH to 1.02 K (0.76–1.62) at 100 ATH.

Figure 16 illustrates the resulting cooling effect for Scenario 2 which combines lower zone temperatures with enhanced air movement. Cooling effect rose from 0.3 K (0.2–0.5) at 10 ATH to 4.8 K (4.4–5.3) at 100 ATH, surpassing Scenario 1 values due to the additional contribution of reduced air and radiant temperatures.

Unlike Scenario 1, the reference temperature difference decreased with increasing ATH, as shown in Figure 17, because operative temperatures were not held constant when compared to its respective no-fan baseline model for Scenario 2. Consistent with Scenario 1, reductions in the reference temperature difference occur when the zone operative temperature decreases, the supply water temperature increases, or when the supply to return water temperature difference increases. Zone area and fan flow direction remained minor factors. Figure 18 shows that the equivalent heat transfer coefficient increased under the same conditions identified in Scenario 1: lower supply water temperature, higher fan speeds, higher operative temperatures, tighter pipe spacing, smaller supply to return water temperature difference, and absence of carpet. Again, zone size and airflow direction had little influence.

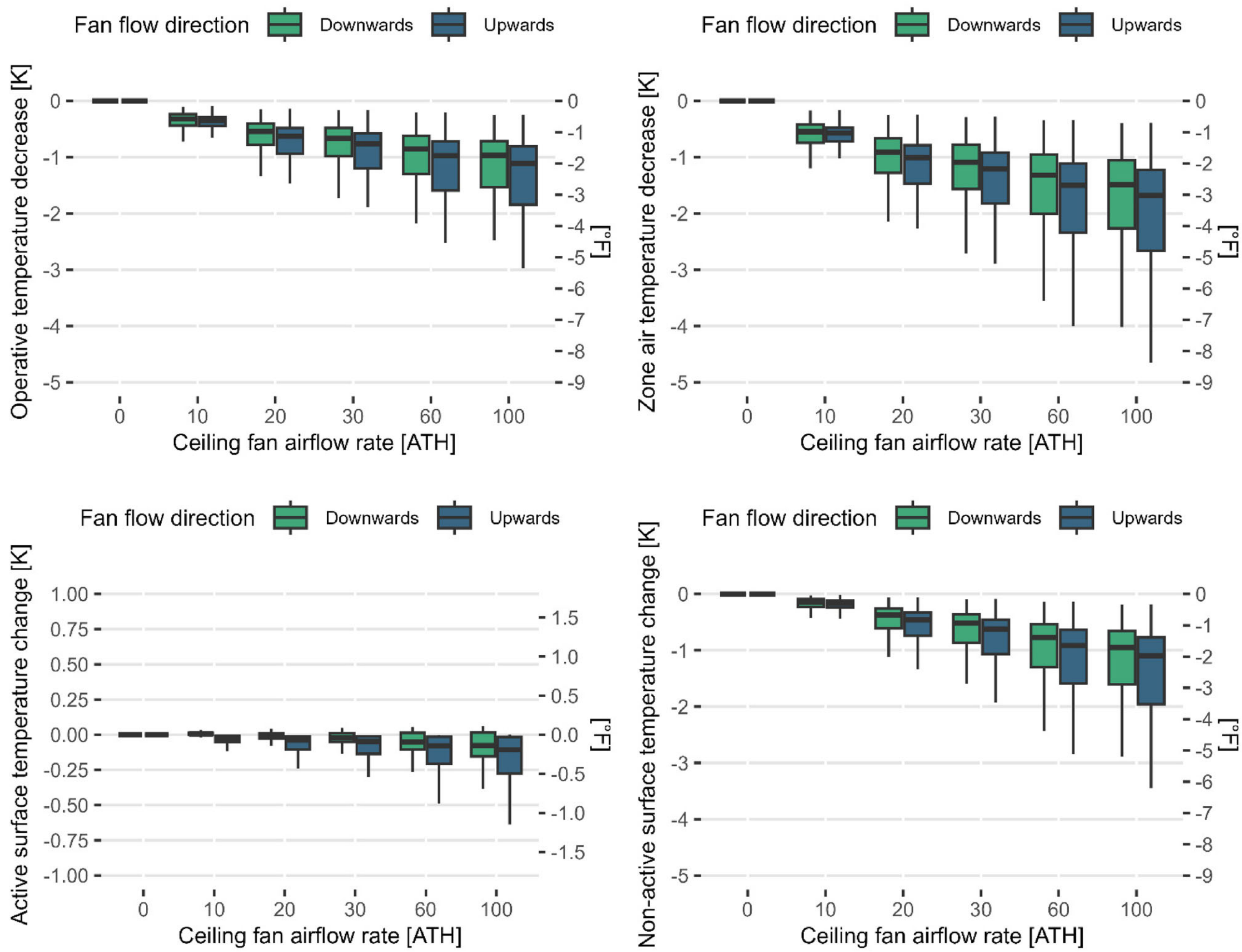

Figure 15. Changes in zone (top-left) operative, (top-right) air, (bottom-left) active surface, and (bottom-right) non-active surface temperatures for various ceiling fan air turnover per hour (ATH) grouped by airflow direction for Scenario 2. Active surface surfaces refer to the ceiling and floor surfaces, e.g. the tubing is embedded in the structural floor/ceiling slab. Non-active surface refers to wall surfaces, e.g. tubing is not embedded within the structure.

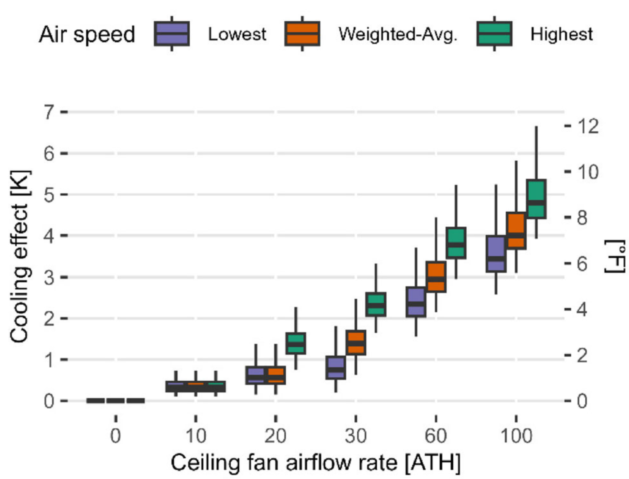

Figure 16. The change in standard effective temperature (SET) to quantify the combined cooling effect of the decrease in zone temperatures and increase in air movement for a seated occupant.

4. Discussion

The simulations in this two-step study explore the effects of increased air movement, induced by ceiling fans, on the performance of thermally activated building radiant cooling systems. The results demonstrate that elevated air movement can substantially increase convective heat transfer coefficients, enhance the cooling heat transfer rate of radiant systems, and provide a significant cooling effect to occupants. These outcomes are consistent with previous studies, which have shown that introducing forced convection through supply diffusers or ceiling fans can increase cooling capacity by 4–37% depending on the scenario. In addition to corroborating these findings, this study extends the research in a couple of ways. First, while much of the literature focuses on forced convection through supply diffusers on radiant panels or

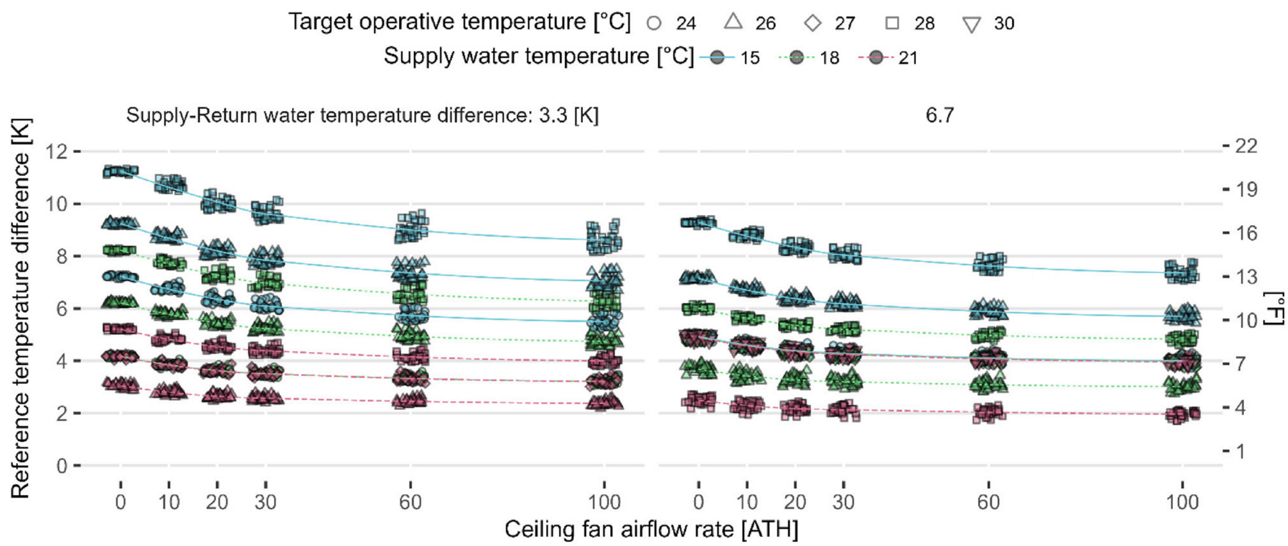

Figure 17. The effect of various design parameters on reference temperature difference (ΔT_h) when we fix the input internal heat gains and radiant system water flow rate as we vary the ceiling fan air turnover per hour (ATH). The target operative temperature is only achieved in baseline models where there are no fans, i.e. the operative temperature decreases as ATH increases. Point jitter is added to the x-direction to help visualize the type and density of points at each ATH.

wall systems, this work addresses TABS coupled with ceiling fans, which differ fundamentally in terms of zone air circulation and thermal inertia, which ultimately affects the thermal dynamics of the system. Second, by deriving simplified regression-based convective models from CFD data and implementing them in EnergyPlus, the study bridges detailed airflow simulations with whole building energy modelling. This approach enables a more systematic exploration of design factors such as ATH, flow direction, operative temperature, and pipe spacing while minimizing computational resources. Additionally, other researchers can directly utilize the simplified regression models to estimate the impacts of ceiling fans in their own unique projects. In the long term, these models can be integrated into modelling and simulation tools such as EnergyPlus and the CBE-Rad Tool (Raftery et al. 2019). Since convection acts as a boundary condition governing heat exchange, the simplified models are not intrinsically limited to hydronic systems. They could also be tested to evaluate their applicability for the interactions between ceiling fans with variable air volume (VAV) systems or for night ventilation strategies aimed at precooling building mass. More broadly, the models could provide a practical framework for rapidly estimating how ceiling fans influence surface convection and system performance across diverse building types and operational contexts. As such, they could represent a valuable starting point for exploring advanced load-shifting strategies leveraging ceiling fans, enabling designers and researchers to assess potential energy, comfort, and grid-interactive benefits with relatively low computational effort before moving to more detailed simulations or field studies.

The results of this study highlight important implications for the design and operation of radiant cooling systems. In Scenario 1, where the operative temperature and supply-return water temperature difference were held constant, ceiling fans increased the steady-state cooling heat transfer rate by 9–47% depending on ATH. This suggests that designers could size radiant systems combined with ceiling fans with more flexibility, reducing the need for supplemental cooling systems. In Scenario 2, where radiant system capacity was fixed, elevated air movement lowered operative temperature by up to 1 K at 100 ATH, providing an additional 4–5 K of cooling effect when combined with the physiological benefits of elevated air speeds in the thermal zone. The results from the two scenarios support the notion that ceiling fans can effectively shift the thermal balance between radiant and convective loads. By enhancing convective transfer at cooled surfaces, fans allow radiant systems to operate with warmer supply water temperatures. Furthermore, the radiant and ceiling fan-coupled system extends the thermal comfort envelope by giving more direct control over three out of six significant factors – air and mean radiant temperatures, and air movement – that affect thermal comfort (ASHRAE 2023). This enables the system to produce neutral thermal sensations at higher operative temperatures. The energy penalty of including ceiling fans is small since fans use 30–50 times less operational energy than HVAC systems (Morris et al. 2021). The overall effect of warmer

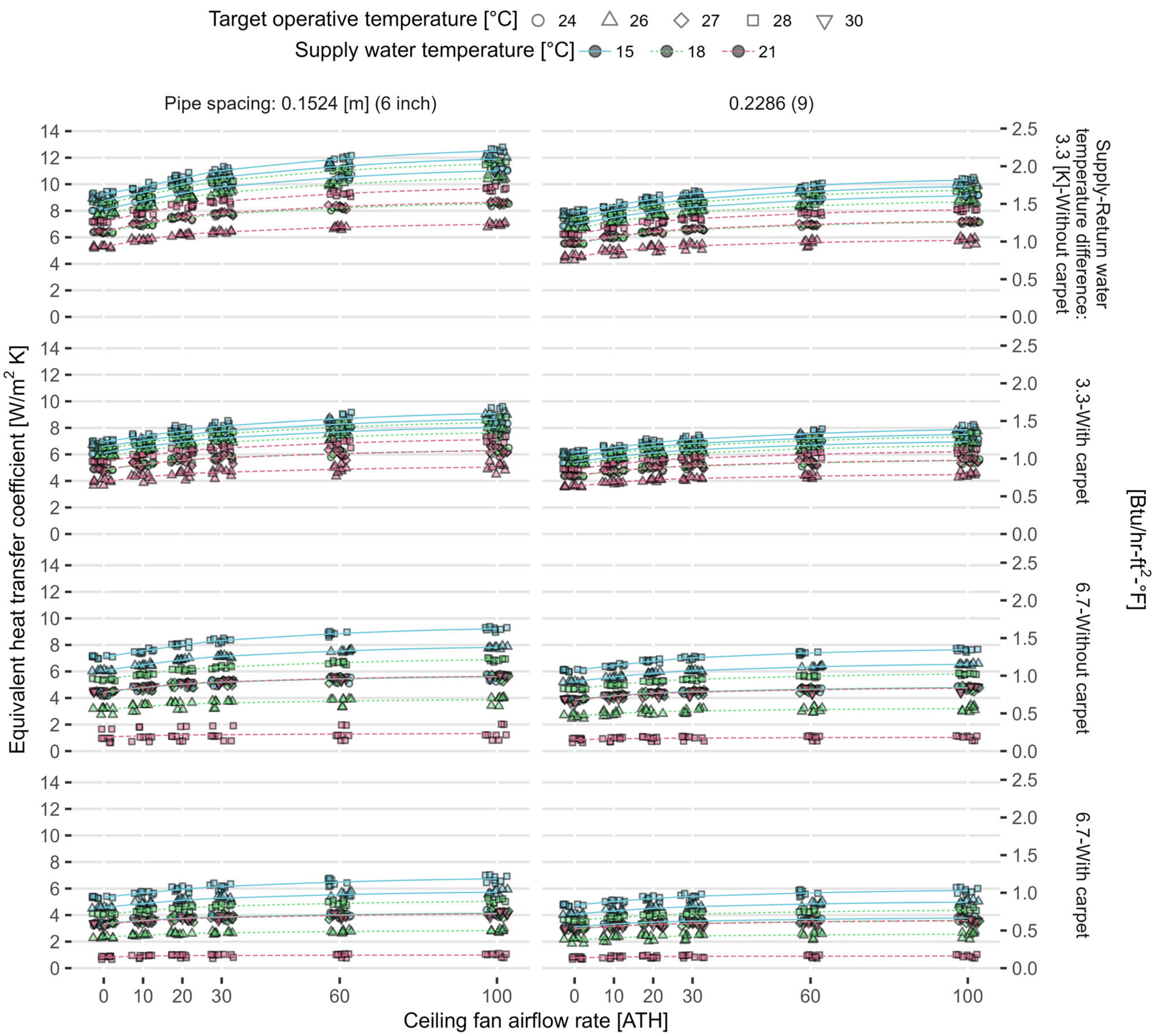

Figure 18. The effect of various design parameters on equivalent heat transfer coefficient (K_H) when we fix the internal heat gains and radiant system water flow rate as we vary the ceiling fan air turnover per hour (ATH). The target operative temperature is only achieved in baseline models where there are no fans. The operative temperature decreases as ATH increases. Point jitter is added to the x-direction to visualize the type and density of points at each ATH.

supply water and zone operative temperatures is a reduction in chiller power demand, improvement in energy efficiency, and the potential to expand the operating range of radiant cooling systems into hotter climates.

This study also examines the fan flow direction which indicates that downward flows most strongly enhance convection at the floor, while upward flows are more effective at the ceiling. This directional sensitivity aligns with physical expectations. That is, downward jets disrupt stagnant boundary layers at cooled floors, whereas upward flows counteract buoyancy effects at cooled ceilings. Directionality also affects the system's total cooling heat transfer rate. The results show that an upward flow can increase the median cooling heat transfer rate of the system by an additional 8% at the maximum ATH evaluated. For designers, this suggests that optimal fan operation strategies may be tailored to the surface type and desired cooling distribution, while keeping in mind that operating in shared spaces can present challenges in satisfying occupants' air movement preferences. A downward flow produces less uniform air speeds, i.e. higher air speeds directly under the fan, while an upward flow can produce more uniform air movement in the space, but the ceiling fans are not always designed to do so, causing lower fan thrust at the same fan rotational speeds when operating in different directions (Raftery, Fizer, et al. 2019). The relatively small differences observed at walls further indicate that ceiling and floor surfaces dominate fan-induced effects.

4.1. Limitations

While the radiant and ceiling-fan coupled system shows promising results, several limitations warrant discussion. First, all simulations were conducted under steady-state conditions. TABS operate dynamically in practice, and their large thermal mass means that transient interaction with fan operation, internal load variations, and control strategies differ from steady-state predictions. Nevertheless, steady-state capacity remains the conventional design basis, and the results are therefore directly relevant for sizing and system integration. Second, the CFD approach modelled fans as thrust forces rather than detailed blade geometries. Laboratory studies suggest this simplification is valid for predicting bulk air movement away from the fan (Raftery, Fizer, et al. 2019), but a fan-specific design may yield local variations not captured here. However, related limitations that can cause larger uncertainty in the results are the exclusion of furniture in the modelling and other obstructions (e.g. exposed ductwork on ceilings) and room configurations (e.g. non-square floor plans, off-centered fans, or differing layout of multiple fans). Airflow rates from ceiling fans can be restricted by furniture and reduce air speeds by up to 0.7 m s^{-1} (Luo et al. 2021) and air flow circulation in other room configurations will not match our modelled room configuration, adding uncertainty to the enhanced convection predictions of this study. Third, condensation was not explicitly modelled, though it remains a critical constraint in radiant cooling. The condensation risk will be affected by elevated air movement, but little research has been conducted to quantify its effect on these types of systems. Our analysis suggests that elevated air movement reduces condensation risk since the same cooling capacity can be achieved with higher room and surface temperatures when compared to the no-fan case. Nevertheless, our analysis assumed proper humidity control by ventilation systems at steady-state and still air conditions, but field implementations must carefully address condensation risks.

Finally, the regression-based convection models derived in this study are more accurate at fan speeds above 10 ATH, as performance at lower levels closely resembles natural convection. This suggests a minimum threshold of air movement is needed before meaningful cooling heat transfer rate gains occur, an important consideration for fan sizing and control.

5. Conclusions

This study examined the influence of elevated air movement on the performance of thermally activated building (TABS) radiant systems using a two-step simulation approach. We first used OpenFOAM, an open-source computational fluid dynamics (CFD) tool, to estimate surface-specific (i.e. floor, ceiling, and wall) convective heat transfer coefficients under varying ceiling fan air turnover rates (ATH) and airflow directions. We utilized the CFD results to derive simplified regression-based models for convective heat transfer coefficients. Then, we integrated the simplified models into single zone whole building energy models to assess the coupled performance of TABS and ceiling fans across a wide range of geometric, operational, and design factors and conditions. We presented two scenarios in the whole building energy simulation analysis.

The results from Scenario 1, where we fixed zone operative temperatures and supply to return water temperature differences, show that elevated air movement increases TABS cooling heat transfer rate from a median 9.5% at 10 ATH to 47% at 100 ATH, with maximum gains approaching 49 W m^{-2}. In Scenario 2, where we fixed baseline system inputs to maintain a constant cooling capacity as the fan ATH varies, ceiling fans reduced operative temperatures and provided occupants with up to 5 K of additional cooling effect. These findings confirm that fan-induced air movement not only augments the steady-state cooling heat transfer rate of radiant systems but also extends their comfort range.

By demonstrating how elevated air movement can significantly improve the performance of TABS, this study contributes directly to the ongoing effort to decarbonize the building sector. Radiant cooling systems already reduce reliance on energy-intensive, low-temperature air systems, but their adoption has often been constrained by perceived limitations in cooling capacity and response time. Coupling these systems with ceiling fans addresses this barrier, enabling higher supply water and zone operative temperatures, reducing cooling power demand, maintaining occupant thermal comfort, and ultimately lowering both energy use and greenhouse gas emissions. These findings suggest that radiant and fan-coupled systems offer a scalable, low-cost strategy for delivering high thermal comfort while advancing net-zero energy and carbon-neutral building targets. As policies and design practices increasingly prioritize grid flexibility and climate resilience, the integration of ceiling fans with radiant cooling represents a practical and impactful design pathway toward the broader decarbonization of the built environment.

Acknowledgements

This research was financially supported by Clark Pacific, a member of the University of California, Berkeley, Center for the Built Environment (CBE) industry consortium.

Author contributions

CRediT: **Carlos Duarte Roa:** Conceptualization, Data curation, Formal analysis, Investigation, Methodology, Software, Supervision, Validation, Visualization, Writing – original draft, Writing – review & editing; **Paul Raftery:** Conceptualization, Funding acquisition, Methodology, Supervision, Validation, Writing – original draft, Writing – review & editing; **Sangjoon Lee:** Formal analysis, Investigation, Methodology, Software, Visualization, Writing – original draft, Writing – review & editing; **Aslihan Senel Solmaz:** Investigation, Writing – original draft, Writing – review & editing

Nomenclature

h_c	Surface convective heat transfer coefficient [W m^{-2} K^{-1}]
w	Zone width [m]
d	Zone depth [m]
h	Zone height [m]
h_f	Ceiling-to-fan distance [m]
d_f	Fan diameter [m]
$A_{s,zone}$	Small zone floor area [m^2]
$A_{l,zone}$	Large zone floor area [m^2]
T	Spatial mean of the zone temperature [°C]
T_{cc}	Zone ceiling surface temperature [°C]
T_{cf}	Zone floor surface temperature [°C]
T_h	Zone vertical wall surface temperature [°C]
T_{wi}	Supply, or inlet, water temperature [°C]
T_{wo}	Return, or outlet, water temperature [°C]
T_{op}	Zone operative temperature [°C]
v_f	Fan air speed [m s^{-1}]
N_f	Number of fans [-]
V_{zone}	Volume of the zone [m^3]
q	Surface heat flux [W m^{-2}]
$q_{ceiling}$	Ceiling surface heat flux [W m^{-2}]
q_{floor}	Floor surface heat flux [W m^{-2}]
q_{wall}	Side wall surface heat flux [W m^{-2}]
ΔT	Temperature difference between mean zone air and surface temperature [K]
ΔT_h	Reference temperature difference [K]
K_H	Equivalent heat transfer coefficient [W m^{-2} K^{-1}]
D_h	Hydraulic diameter of the zone [m]
A	Linear coefficient for the fan air turnover rate term in the surface convective heat transfer model [-]
B	Linear coefficient for the temperature difference in the surface convective heat transfer model [-]
G	Linear coefficient for the zone hydraulic diameter in the surface convective heat transfer model [-]
C	Constant term in the surface convective heat transfer model [W m^{-2} K^{-1}]
α	Exponential coefficient for the fan air turnover rate term in the surface convective heat transfer model [-]
β	Exponential coefficient for the temperature difference in the surface convective heat transfer model [-]
γ	Exponential coefficient for the zone hydraulic diameter in the surface convective heat transfer model [-]

Disclosure statement

No potential conflict of interest was reported by the author(s).

Funding

This work was supported by Clark Pacific.

Declaration of generative AI and AI-assisted technologies

During the preparation of this work, the authors used Grammarly and ChatGPT 5 in order to improve language, readability, and writing style. After using these tools, the authors reviewed and edited the content as needed and take full responsibility for the content of the publication.

Data availability statement

The authors confirm that the data supporting the findings of this study are available within the article and its supplementary materials.

ORCID

Carlos Duarte Roa http://orcid.org/0000-0002-5129-2969
Paul Raftery https://orcid.org/0000-0002-6532-5178

References

Arumugam, J., M. P. Maiya, and S. M. Shiva Nagendra. 2024. "Experimental Evaluation of Thermal Characteristics of Wall Mounted Radiant Cooled Environment with Ceiling Fan." *Sādhanā* 49 (2): 119. https://doi.org/10.1007/s12046-024-02480-5.

ASHRAE. 2023. *ASHRAE Standard 55-2023: Thermal Environmental Conditions for Human Occupancy*. Atlanta, GA: American Society of Heating, Refrigerating and Air Conditioning Engineers Inc.

Babiak, J., B. Olesen, and D. Petras. 2009. *REHVA Guidebook No. 7: Low Temperature Heating and High Temperature Cooling*. Brussels, Belgium: Federation of European Heating and Air-Conditioning Associations.

Babich, F., M. Cook, D. Loveday, R. Rawal, and Y. Shukla. 2017. "Transient Three-dimensional CFD Modelling of Ceiling

Fans." *Building and Environment* 123:37–49. https://doi.org/10.1016/j.buildenv.2017.06.039.

Bauman, F., P. Raftery, S. Schiavon, C. Karmann, J. Pantelic, C. Duarte, J. Woolley, et al. 2019. *Optimizing Radiant Systems for Energy Efficiency and Comfort* (No. EPC-14-009). Sacramento, CA: California Energy Commission.

Carnieletto, L., O. B. Kazanci, B. W. Olesen, A. Zarrella, and W. Pasut. 2024. "Combining Energy Generation and Radiant Systems: Challenges and Possibilities for Plus Energy Buildings." *Energy and Buildings* 325:114965. https://doi.org/10.1016/j.enbuild.2024.114965.

Causone, F., S. P. Corgnati, M. Filippi, and B. W. Olesen. 2009. "Experimental Evaluation of Heat Transfer Coefficients between Radiant Ceiling and Room." *Energy and Buildings* 41 (6): 622–628. https://doi.org/10.1016/j.enbuild.2009.01.004.

Chantrasrisalai, C., V. Ghatti, D. E. Fisher, and D. G. Scheatzle. 2003. "Experimental Validation of the EnergyPlus Low-Temperature Radiant Simulation." *ASHRAE Transactions* 109 (2): 614–623.

Chen, W., S. Liu, Y. Gao, H. Zhang, E. Arens, L. Zhao, and J. Liu. 2018. "Experimental and Numerical Investigations of Indoor air Movement Distribution with an Office Ceiling fan." *Building and Environment* 130:14–26. https://doi.org/10.1016/j.buildenv.2017.12.016.

Crawley, Drury B., and L. K. Lawrie. 1999. EnergyPlus: A New-Generation Building Energy Simulation.

Duarte Roa, C., P. Raftery, S. Schiavon, and F. Bauman. 2025. "How High Can You Go: Determining the Warmest Supply Water Temperature for High Thermal Mass Radiant Cooling Systems under Thermal Comfort Constraints." *Energy and Buildings* 331:115387. https://doi.org/10.1016/j.enbuild.2025.115387.

Geuzaine, C., and J.-F. Remacle. 2009. "Gmsh: A 3-D Finite Element Mesh Generator with Built-in Pre- and Post-processing Facilities." *International Journal for Numerical Methods in Engineering* 79 (11): 1309–1331. https://doi.org/10.1002/nme.2579.

Geuzaine, C., and J.-F. Remacle. 2022. Gmsh (Version 4.11.1).

Gray, D. D., and A. Giorgini. 1976. "The Validity of the Boussinesq Approximation for Liquids and Gases." *International Journal of Heat and Mass Transfer* 19 (5): 545–551. https://doi.org/10.1016/0017-9310(76)90168-X.

Greenshields, C. 2023. *OpenFOAM v11 User Guide*. London: The OpenFOAM Foundation.

Guo, X., S. Wan, W. Chen, H. Zhang, E. Arens, Y. Cheng, and W. Pasut. 2023. "Numerical Simulation of Cooling Performance of Radiant Ceiling System Interacting with a Ceiling Fan." *Energy and Buildings* 297:113492. https://doi.org/10.1016/j.enbuild.2023.113492.

Gwerder, M., B. Lehmann, J. Tödtli, V. Dorer, and F. Renggli. 2008. "Control of Thermally-Activated Building Systems (TABS)." *Applied Energy* 85 (7): 565–581. https://doi.org/10.1016/j.apenergy.2007.08.001.

He, Y., W. Chen, Z. Wang, and H. Zhang. 2019. "Review of Fan-use Rates in Field Studies and Their Effects on Thermal Comfort, Energy Conservation, and Human Productivity." *Energy and Buildings* 194:140–162. https://doi.org/10.1016/j.enbuild.2019.04.015.

Henninger, R. H., M. J. Witte, and D. B. Crawley. 2004. "Analytical and Comparative Testing of EnergyPlus Using IEA HVAC BESTEST E100–E200 Test Suite." *Energy and Buildings* 36 (8): 855–863. https://doi.org/10.1016/j.enbuild.2004.01.025.

Higgins, C., and K. Carbonnier. 2017. *Energy Performance of Commercial Buildings with Radiant Heating and Cooling*. Portland, OR: New Buildings Institute.

ISO. 2021. *ISO 11855:2021 - building Environment Design-design, Dimensioning, Installation and Control of Embedded Radiant Heating and Cooling Systems*. Geneva, Switzerland: International Organization for Standardization.

Jeong, J.-W., and S. A. Mumma. 2003. "Ceiling Radiant Cooling Panel Capacity Enhanced by Mixed Convection in Mechanically Ventilated Spaces." *Applied Thermal Engineering* 23 (18): 2293–2306. https://doi.org/10.1016/S1359-4311(03)00211-4.

Karmann, C., F. Bauman, P. Raftery, S. Schiavon, and M. Koupriyanov. 2018. "Effect of Acoustical Clouds Coverage and Air Movement on Radiant Chilled Ceiling Cooling Capacity." *Energy and Buildings* 158:939–949. https://doi.org/10.1016/j.enbuild.2017.10.046.

Kent, M. G., N. K. Huynh, A. K. Mishra, F. Tartarini, A. Lipczynska, J. Li, Z. Sultan, et al. 2023. "Energy Savings and Thermal Comfort in a Zero Energy Office Building with Fans in Singapore." *Building and Environment* 243:110674. https://doi.org/10.1016/j.buildenv.2023.110674.

Luo, M., H. Zhang, P. Raftery, L. Zhou, T. Parkinson, E. Arens, Y. He, and E. Present. 2021. "Detailed Measured Air Speed Distribution in Four Commercial Buildings with Ceiling Fans." *Building and Environment* 200:107979. https://doi.org/10.1016/j.buildenv.2021.107979.

Menter, F. R., M. Kuntz, and R. Langtry. 2003. "Ten Years of Industrial Experience with the SST Turbulence Model." *Turbulence, Heat and Mass Transfer* 4 (1): 625–632.

Miller, D., P. Raftery, M. Nakajima, S. Salo, L. T. Graham, T. Peffer, M. Delgado, et al. 2021. "Cooling Energy Savings and Occupant Feedback in a Two Year Retrofit Evaluation of 99 Automated Ceiling Fans Staged with Air Conditioning." *Energy and Buildings* 251:111319. https://doi.org/10.1016/j.enbuild.2021.111319.

Moftakhari, A., S. Bourne, and A. Novoselac. 2023. "All-air vs. Radiant Cooling Systems: Analysis of Design and Operation Factors That Impact Building Cooling Loads (ASHRAE RP 1729)." *Science and Technology for the Built Environment* 29 (4): 381–401. https://doi.org/10.1080/23744731.2023.2183016.

Morris, N. B., G. K. Chaseling, T. English, F. Gruss, M. F. B. Maideen, A. Capon, and O. Jay. 2021. "Electric Fan Use for Cooling during Hot Weather: A Biophysical Modelling Study." *The Lancet Planetary Health* 5 (6): e368–e377. https://doi.org/10.1016/S2542-5196(21)00136-4.

Mosa, M., M. Labat, and S. Lorente. 2019. "Role of Flow Architectures on the Design of Radiant Cooling Panels, a Constructal Approach." *Applied Thermal Engineering* 150:1345–1352. https://doi.org/10.1016/j.applthermaleng.2018.12.107.

Nevers, C., M. Labat, and A. Malley-Ernewein. 2025. "Cooling Peak Load Reduction Potential of Ventilated Slabs: A Numerical Study." *Journal of Building Performance Simulation* 18 (2): 136–160. https://doi.org/10.1080/19401493.2024.2428732.

Novoselac, A., B. J. Burley, and J. Srebric. 2006. "New Convection Correlations for Cooled Ceiling Panels in Room with Mixed and Stratified Airflow." *HVAC&R Research* 12 (2): 279–294. https://doi.org/10.1080/10789669.2006.10391179.

Olesen, B. W. 1997. "Possibilities and Limitations of Radiant Floor Cooling." *ASHRAE Transactions* 103 (1): 42–48.

Pantelic, J., S. Schiavon, B. Ning, E. Burdakis, P. Raftery, and F. Bauman. 2018. "Full Scale Laboratory Experiment on the Cooling

Capacity of a Radiant Floor System." *Energy and Buildings* 170:134–144. https://doi.org/10.1016/j.enbuild.2018.03.002.

Park, B., and M. Krarti. 2019. "Optimal Control Strategies for Hollow Core Ventilated Slab Systems." *Journal of Building Engineering* 24:100762. https://doi.org/10.1016/j.jobe.2019.100762.

Raftery, P. 2019. *CBE Fan Tool. Berkeley, CA: Center for the Built Environment*. Berkeley, CA: University of California Berkeley.

Raftery, P., and D. Douglass-Jaimes. 2020. *Ceiling Fan Design Guide*. Berkeley, CA: Center for the Built Environment.

Raftery, P., C. Duarte, S. Schiavon, and F. Bauman. 2017. "A New Control Strategy for High Thermal Mass Radiant Systems." In *Proceedings of Building Simulation 2017*, edited by Charles S. Barnaby and Michael Wetter, 755–764. San Francisco, CA: International Building Performance Simulation Association. https://doi.org/10.26868/25222708.2017.192.

Raftery, P., C. Duarte Roa, S. Yang, S. Schiavon, and F. Bauman. 2019. *CBE Rad Tool. Berkeley, CA: Center for the Built Environment*. Berkeley, CA: University of California Berkeley.

Raftery, P., J. Fizer, W. Chen, Y. He, H. Zhang, E. Arens, S. Schiavon, and G. Paliaga. 2019. "Ceiling Fans: Predicting Indoor Air Speeds Based on Full Scale Laboratory Measurements." *Building and Environment* 155:210–223. https://doi.org/10.1016/j.buildenv.2019.03.040.

Rhee, K.-N., and K. W. Kim. 2015. "A 50 Year Review of Basic and Applied Research in Radiant Heating and Cooling Systems for the Built Environment." *Building and Environment* 91:166–190. https://doi.org/10.1016/j.buildenv.2015.03.040.

Shindo, K., K. Ikai, J. Shinoda, R. Matsumura, and S. Tanabe. 2024. "Design and Control of Radiant Heating and Cooling Systems in Japan: Results from Expert Interviews." *Japan Architectural Review* 7 (1): e12451. https://doi.org/10.1002/2475-8876.12451.

Shindo, K., J. Shinoda, O. B. Kazanci, D.-I. Bogatu, S. Tanabe, and B. W. Olesen. 2023. "A Comparative Study of the Whole Life Carbon of a Radiant System and an All-air System in a Non-residential Building." *Energy and Buildings* 300:113668. https://doi.org/10.1016/j.enbuild.2023.113668.

Shinoda, J., O. B. Kazanci, S. Tanabe, and B. W. Olesen. 2019. "A Review of the Surface Heat Transfer Coefficients of Radiant Heating and Cooling Systems." *Building and Environment* 159:106156. https://doi.org/10.1016/j.buildenv.2019.05.034.

Tanabe, S., and K. Kimura. 1994. "Effects of Air Temperature, Humidity, and Air Movement on Thermal Comfort under Hot and Humid Conditions." *ASHRAE Transactions* 100:953–969.

Uponor. 2013. *Radiant Cooling Design Manual: Embedded Systems for Commercial Applications (First)*. Minnesota: Uponor, Inc.

Venko, S., D. Vidal de Ventós, C. Arkar, and S. Medved. 2014. "An Experimental Study of Natural and Mixed Convection over Cooled Vertical Room Wall." *Energy and Buildings* 68:387–395. https://doi.org/10.1016/j.enbuild.2013.09.014.

Zeytounian, R. K. 2003. "Joseph Boussinesq and His Approximation: A Contemporary View." *Comptes Rendus. Mécanique* 331 (8): 575–586. https://doi.org/10.1016/S1631-0721(03)00120-7.

Zmeureanu, R., and P. Fazio. 1988. "Thermal Performance of a Hollow Core Concrete Floor System for Passive Cooling." *Building and Environment* 23 (3): 243–252. https://doi.org/10.1016/0360-1323(88)90009-1.

Appendix

Table A1. Ceiling, floor, and wall surface convective heat transfer coefficients estimations using the models developed with equation 5 and equation parameters listed in Table 3. The estimations are for a large zone (500 m^2) for various ceiling fan air turnover per hour (ATH), fan flow direction, and temperature difference between the mean zone air and zone surface. Note that estimations for natural convection (ATH $= 0$) are derived from the ASHRAE guidelines and included in table for reference.

Surface	Fan flow direction	Air turnover per hour (ATH)	*Air-Surface* $\Delta T = 0.1\,K$	0.25	0.5	1	1.5	2	3	4	6	8	10
ceiling	downwards	0	0.92	1.23	1.52	1.89	2.14	2.34	2.65	2.9	3.29	3.6	3.85
		10	2.15	2.46	2.71	2.97	3.14	3.25	3.43	3.56	3.74	3.88	3.98
		20	3.26	3.56	3.82	4.08	4.24	4.36	4.54	4.67	4.85	4.99	5.09
		30	4.1	4.41	4.66	4.92	5.09	5.21	5.38	5.51	5.69	5.83	5.94
		60	5.98	6.29	6.54	6.8	6.97	7.09	7.26	7.39	7.57	7.71	7.81
		100	7.82	8.13	8.38	8.65	8.81	8.93	9.1	9.23	9.42	9.55	9.66
	upwards	10	2.88	3.1	3.27	3.45	3.56	3.64	3.75	3.83	3.94	4.02	4.09
		20	4.82	5.04	5.21	5.39	5.5	5.58	5.69	5.77	5.88	5.96	6.03
		30	6.37	6.59	6.76	6.94	7.04	7.12	7.23	7.31	7.43	7.51	7.57
		60	9.99	10.21	10.39	10.57	10.67	10.75	10.86	10.94	11.05	11.14	11.2
		100	13.75	13.97	14.14	14.32	14.43	14.51	14.62	14.7	14.81	14.89	14.96
floor	downwards	0	0.05	0.07	0.08	0.09	0.1	0.11	0.12	0.13	0.14	0.15	0.16
		10	2.1	2.13	2.15	2.17	2.18	2.18	2.19	2.2	2.21	2.22	2.23
		20	3.73	3.75	3.77	3.79	3.8	3.81	3.82	3.83	3.84	3.84	3.85
		30	5.19	5.21	5.23	5.25	5.26	5.27	5.28	5.29	5.3	5.3	5.31
		60	9.08	9.1	9.12	9.14	9.15	9.16	9.17	9.18	9.19	9.19	9.2
		100	13.67	13.7	13.72	13.74	13.75	13.76	13.77	13.78	13.79	13.79	13.8
	upwards	10	0.87	0.83	0.81	0.78	0.77	0.76	0.74	0.73	0.72	0.71	0.7
		20	1.68	1.65	1.62	1.6	1.58	1.57	1.56	1.55	1.54	1.53	1.52
		30	2.44	2.41	2.39	2.36	2.35	2.34	2.32	2.31	2.3	2.29	2.28
		60	4.57	4.53	4.51	4.48	4.47	4.46	4.45	4.43	4.42	4.41	4.4
		100	7.19	7.16	7.13	7.11	7.09	7.08	7.07	7.06	7.04	7.03	7.03
wall	downwards	0	0.85	1.14	1.43	1.78	2.03	2.22	2.53	2.77	3.16	3.46	3.72
		10	4.1	4.47	4.75	5.04	5.21	5.34	5.52	5.65	5.83	5.96	6.06
		20	6.97	7.33	7.62	7.91	8.08	8.21	8.38	8.51	8.7	8.83	8.93
		30	9.34	9.7	9.99	10.28	10.45	10.58	10.76	10.88	11.07	11.2	11.3
		60	15.13	15.49	15.78	16.07	16.24	16.37	16.55	16.67	16.86	16.99	17.09
		100	21.38	21.75	22.03	22.32	22.49	22.62	22.8	22.93	23.11	23.24	23.34
	upwards	10	3.64	3.84	3.99	4.15	4.25	4.31	4.41	4.48	4.58	4.65	4.7
		20	6.48	6.68	6.83	6.99	7.08	7.15	7.25	7.31	7.41	7.48	7.54
		30	8.83	9.03	9.19	9.34	9.44	9.51	9.6	9.67	9.77	9.84	9.9
		60	14.62	14.82	14.97	15.13	15.23	15.29	15.39	15.46	15.56	15.63	15.68
		100	20.9	21.1	21.25	21.41	21.51	21.57	21.67	21.74	21.84	21.91	21.96